Atmospheric CH4 in the first decade of the 21st century

Bergamaschi, P.; Houweling, S.; Segers, A.; Krol, M.; Frankenberg, C.; Scheepmaker, R. A.; Dlugokencky, E.; Wofsy, S. C.; Kort, E. A.; Sweeney, C.

Published in:
Journal of geophysical research-Atmospheres

DOI:
10.1002/jgrd.50480

Publication date:
2013

Atmospheric CH_4 in the first decade of the 21st century: Inverse modeling analysis using SCIAMACHY satellite retrievals and NOAA surface measurements

P. Bergamaschi,[1] S. Houweling,[2,3] A. Segers,[1,4] M. Krol,[2,3,5] C. Frankenberg,[6] R. A. Scheepmaker,[2] E. Dlugokencky,[7] S. C. Wofsy,[8] E. A. Kort,[6] C. Sweeney,[7,9] T. Schuck,[10] C. Brenninkmeijer,[10] H. Chen,[7,9,11] V. Beck,[12] and C. Gerbig[12]

Received 30 January 2013; revised 4 May 2013; accepted 7 May 2013; published 1 July 2013.

[1] The causes of renewed growth in the atmospheric CH_4 burden since 2007 are still poorly understood and subject of intensive scientific discussion. We present a reanalysis of global CH_4 emissions during the 2000s, based on the TM5-4DVAR inverse modeling system. The model is optimized using high-accuracy surface observations from NOAA ESRL's global air sampling network for 2000–2010 combined with retrievals of column-averaged CH_4 mole fractions from SCIAMACHY onboard ENVISAT (starting 2003). Using climatological OH fields, derived global total emissions for 2007–2010 are 16–20 Tg CH_4/yr higher compared to 2003–2005. Most of the inferred emission increase was located in the tropics (9–14 Tg CH_4/yr) and mid-latitudes of the northern hemisphere (6–8 Tg CH_4/yr), while no significant trend was derived for Arctic latitudes. The atmospheric increase can be attributed mainly to increased anthropogenic emissions, but the derived trend is significantly smaller than estimated in the EDGARv4.2 emission inventory. Superimposed on the increasing trend in anthropogenic CH_4 emissions are significant inter-annual variations (IAV) of emissions from wetlands (up to $\pm$10 Tg CH_4/yr), and biomass burning (up to $\pm$7 Tg CH_4/yr). Sensitivity experiments, which investigated the impact of the SCIAMACHY observations (versus inversions using only surface observations), of the OH fields used, and of *a priori* emission inventories, resulted in differences in the detailed latitudinal attribution of CH_4 emissions, but the IAV and trends aggregated over larger latitude bands were reasonably robust. All sensitivity experiments show similar performance against independent shipboard and airborne observations used for validation, except over Amazonia where satellite retrievals improved agreement with observations in the free troposphere.

Citation: Bergamaschi, P., et al. (2013), Atmospheric CH_4 in the first decade of the 21st century: Inverse modeling analysis using SCIAMACHY satellite retrievals and NOAA surface measurements, *J. Geophys. Res. Atmos.*, *118*, 7350–7369, doi:10.1002/jgrd.50480.

1. Introduction

[2] Atmospheric methane (CH_4) is the most important anthropogenic greenhouse gas (GHG) after carbon dioxide (CO_2), contributing 18% (0.51 W m^{-2}) of the direct radiative forcing in 2011 due to the increase of long-lived greenhouse gases since preindustrial times (~1750) (update of *Hofmann et al.* [2006]; http://www.esrl.noaa.gov/gmd/aggi/). Taking into account additional indirect effects, CH_4 contributes ~30% of the emission-based radiative forcing [*Forster et al.*, 2007; *Shindell et al.*, 2005]. Owing to its relatively short atmo-

Additional supporting information may be found in the online version of this article.

[1]Institute for Environment and Sustainability, Joint Research Centre, European Commission, Ispra, Italy.
[2]SRON Netherlands Institute for Space Research, Utrecht, Netherlands.
[3]Institute for Marine and Atmospheric Research Utrecht (IMAU), Utrecht, Netherlands.
[4]Netherlands Organisation for Applied Scientific Research (TNO), Utrecht, Netherlands.
[5]Meteorology and Air Quality Department, Wageningen University and Research Centre, Wageningen, Netherlands.
[6]Jet Propulsion Laboratory, California Institute of Technology, Pasadena, California, USA.
[7]Global Monitoring Division, NOAA Earth System Research Laboratory, Boulder, Colorado, USA.
[8]School of Engineering and Applied Science and Department of Earth and Planetary Sciences, Harvard University, Cambridge, Massachusetts, USA.
[9]CIRES, University of Colorado, Boulder, Colorado, USA.
[10]Max Planck Institute for Chemistry, Mainz, Germany.
[11]Center for Isotope Research, University of Groningen, Groningen, Netherlands.
[12]Max Planck Institute for Biogeochemistry, Jena, Germany.

Corresponding author: P. Bergamaschi, Institute for Environment and Sustainability, Joint Research Centre, European Commission, Ispra, Italy. (peter.bergamaschi@jrc.ec.europa.eu)

2169-897X/13/10.1002/jgrd.50480

spheric lifetime of ~10 years, atmospheric CH_4 is an attractive target to mitigate climate change over the next few decades [*Shindell et al*., 2012]. At the same time, however, natural CH_4 sources have the potential to significantly amplify human-induced climate change on long timescales (centuries to millennia) due to significant dependence of CH_4 wetland emissions on climate, melting of permafrost, and potential destabilization of CH_4 hydrates [e.g., *Brook et al*., 2008; *Shakhova et al*., 2010; *Walter Anthony et al*., 2012].

[3] Measurements of air trapped in polar firn and ice cores show that contemporary atmospheric CH_4 is 2.5 times higher than that in preindustrial times (~1750) [*Etheridge et al*., 1998] and unprecedented during the last 800,000 years [*Loulergue et al*., 2008; *Spahni et al*., 2005]. Atmospheric CH_4 has been measured directly since the late 1970s [*Blake and Rowland*, 1988; *Cunnold et al*., 2002; *Dlugokencky et al*., 1994a, 2011]. The observations show that CH_4 was increasing through the 1980s and 1990s, but the rate of increase was decreasing. During 1999–2006, atmospheric CH_4 stabilized [*Dlugokencky et al*., 2003; *Simpson et al*., 2006], but it started to rise again significantly since 2007 [*Dlugokencky et al*., 2009; *Rigby et al*., 2008]. The slowdown in growth rate during the 1980s and 1990s and the leveling-off beginning in 1999 was interpreted by *Dlugokencky et al*. [2003] as approach to steady state with approximately constant CH_4 total emissions and CH_4 lifetime, while *Bousquet et al*. [2006] derived from an atmospheric inversion decreasing anthropogenic emissions in the 1990s and decreasing wetland emissions in the 2000s, masking a renewed increase of anthropogenic emissions. *Aydin et al*. [2011] and *Simpson et al*. [2012] suggested decreasing emissions from fossil sources (based on atmospheric ethane mixing ratios and methane/ethane emission ratios), contrary to bottom-up emission inventories. In contradiction to the studies of *Aydin et al*. [2011] and *Simpson et al*. [2012], *Kai et al*. [2011] had proposed decreasing emissions from microbial sources, most likely from rice agriculture, and excluded reduced fossil fuel emissions as the primary cause of the slowdown, based on measurements of the interhemispheric difference in $\delta^{13}C$-CH_4. However, their conclusion was not confirmed by *Levin et al*. [2012], using independent and more comprehensive $\delta^{13}C$-CH_4 measurements.

[4] Also, the renewed growth of atmospheric CH_4 since 2007 is poorly understood. *Dlugokencky et al*. [2009, 2011] suggested that this increase is mainly meteorologically driven, with anomalously high temperatures in the Arctic in 2007 and greater than average precipitation in the tropics in 2007 and 2008. At the same time, the Emission Database for Global Atmospheric Research version 4.2 (EDGARv4.2) emission time series until 2008 [*JRC/PBL*, 2011] suggests significant increases in anthropogenic CH_4 emissions, albeit increasing also during 2000–2007. *Rigby et al*. [2008] derived a decrease of $4 \pm 14\%$ in globally averaged OH between 2006 and 2007, which could have contributed to the CH_4 increase in 2007, but considered the estimated OH decrease as not significant. The ensuing monitoring of atmospheric CH_4 shows its increase to continue, at an average rate of 6.0 ± 0.9 ppb/yr during 2007–2010 (update of global means from *Dlugokencky et al*. [2009]).

[5] In this paper, we present an inverse-modeling-based reanalysis of global CH_4 emissions during the past decade (2000–2010). The main objective is to better quantify the major geographical regions and source categories responsible for the interannual variation (IAV) and trends during this period. In addition to high-accuracy surface observations from the NOAA Earth System Research Laboratory (ESRL) global cooperative air sampling network, we use also CH_4 satellite retrievals from the Scanning Imaging Absorption Spectrometer for Atmospheric Chartography (SCIAMACHY) instrument on board Envisat, available from 2003 to beginning of 2012. The SCIAMACHY CH_4 data are the first spaceborne measurements which are sensitive to the boundary layer (BL), providing significant constraints on surface emissions especially in tropical regions, which are poorly monitored by the surface network [*Bergamaschi et al*., 2009; *Frankenberg et al*., 2006, 2008]. Although a severe degradation of the detector pixels used for the CH_4 retrievals occurred late 2005, *Frankenberg et al*. [2011] showed that SCIAMACHY CH_4 time series can be obtained that are consistent with the CH_4 trends measured at the NOAA surface sites.

[6] The CH_4 inversions we present include various sensitivity experiments that investigate the impact of (1) the SCIAMACHY observations (compared to inversions using only surface observations), (2) the applied a priori emission inventories, (3) the photochemical sinks, and (4) the bias correction of the SCIAMACHY data on the derived trends and interannual variability of CH_4 emissions. Finally, we present a detailed validation of simulated CH_4 mixing ratios, using NOAA shipboard and aircraft profile samples during the whole target period, CARIBIC (Civil Aircraft for the Regular Investigation of the atmosphere Based on an Instrument Container) aircraft data since mid-2005, HIPPO (High-performance Instrumented Airborne Platform for Environmental Research (HIAPER) Pole-to-Pole Observations) aircraft transects, performed in 2009 and 2010, and aircraft data over the Amazon from the BARCA (Balanço Atmosférico Regional de Carbono na Amazônia) campaigns (2008 and 2009).

2. Observations

2.1. Assimilated Observations

2.1.1. SCIAMACHY Retrievals

[7] In this study, we use CH_4 retrievals from SCIAMACHY (Iterative Maximum A Posteriori version 5.5 (IMAPv5.5)) [*Frankenberg et al*., 2011], including further updates described below. These retrievals are based on the so-called proxy method, using CO_2 as proxy for the total column of the probed atmosphere, and modeled CO_2 fields from CarbonTracker [*Peters et al*., 2007] to account for variations in atmospheric CO_2 [*Frankenberg et al*., 2006, 2011]. The previous Iterative Maximum A Posteriori version 5.0 (IMAPv5.0) [*Frankenberg et al*., 2008] is available only until the end of 2005, when a serious degradation of the detector pixels within the methane 2ν3 absorption band occurred. The new IMAPv5.5 retrievals minimize the impact of the pixel degradation by applying a coherent, uniform pixel mask over the entire period [*Frankenberg et al*., 2011], providing consistent retrievals from 2003 until SCIAMACHY became dysfunctional in April 2012 (when Envisat stopped operating). Although the pixel degradation remains visible in the IMAPv5.5 retrievals as significantly higher noise of the retrievals from November 2005 onward, the retrievals show relatively good consistency over the entire time period as

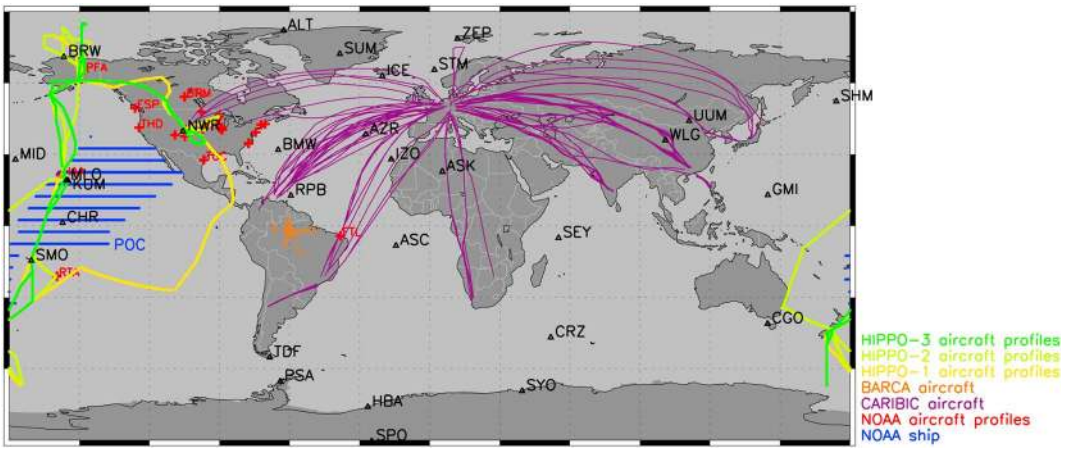

Figure 1. Map showing the locations of NOAA surface sampling sites used in the inversions. Furthermore, the regions of NOAA ship cruises (POC, blue lines, indicating the longitudinal range within each 5° latitude band), the locations of NOAA aircraft profiles, and the flight tracks of CARIBIC (since mid-2005), HIPPO-1 to HIPPO-3 transects (performed in 2009 and 2010), and BARCA-A/BARCA-B campaigns (2008/2009), which are used for validation, are shown.

demonstrated by comparison with the IAV observed at NOAA surface sites [*Frankenberg et al*., 2011]. A drawback of the IMAPv5.5 retrievals, however, is their somewhat reduced quality and some systematic differences compared to the previous IMAPv5.0 retrieval version [*Frankenberg et al*., 2011], resulting in overall larger bias corrections (see sections 3.2 and 4.2) compared to inversions of the IMAPv5.0 retrievals [*Bergamaschi et al*., 2009]. In this study, we used a reprocessed version of the IMAPv5.5 retrievals, including CarbonTracker CO_2 fields for 2008 and 2009 (from CarbonTracker release 2010; http://carbontracker.noaa.gov) for the CO_2 correction, while for 2010 and 2011, non-optimized CO_2 fields were used (based on Tracer Model, version 5 (TM5) forward runs using optimized CO_2 emissions from the previous years) (A. Jacobson, personal communication, 2012).

[8] We apply the same selection criteria as in *Frankenberg et al*. [2011] for the retrievals but use only pixels over land between 50°S and 50°N. Furthermore, we apply a height filter, using only those pixels for which the difference between the surface elevation of the SCIAMACHY pixel and the TM5 model surface is smaller than 250 m [see also *Bergamaschi et al*., 2009].

2.1.2. Surface Observations

[9] Surface observations of CH_4 dry air mole fractions are from the NOAA Earth System Research Laboratory (ESRL) global cooperative air sampling network [*Dlugokencky et al*., 1994b, 2003, 2009]. In this study we use a subset of 30 sites (see Figure 1 and Table S1 in the supporting information), including only marine and continental background sites, omitting sites which are difficult to simulate with the coarse horizontal (6° × 4°) resolution of the TM5 version used (e.g., some coastal sites or sites which are significantly influenced by regional sources). Furthermore, only sites that have a good data coverage over the 2000–2010 inversion period are used. Measurements are reported as dry air mole fractions (denoted "mixing ratios" throughout this paper) in nmol mol^{-1} (abbreviated ppb), calibrated against the NOAA2004 CH_4 standard scale (also the World Meteorological Organization, Global Atmosphere Watch CH_4 mole fraction scale) [*Dlugokencky et al*., 2005].

2.2. Observations Used for Validation

[10] Various data sets have been used to validate the simulated 3-D CH_4 mixing ratios. Not having been used in the inversions, they serve as an independent check of the quality of the simulations. The focus of this validation is on the period 2003–2010, the time span shared by all inversions. NOAA ESRL measurements of discrete air samples taken during regular ship cruises through the Pacific Ocean (POC) are available for the entire 2003–2010 period and serve to validate simulated CH_4 mixing ratios at the surface over the remote ocean and downwind of continental sources. Furthermore, we use NOAA regular aircraft-based vertical profiles to validate the simulated vertical gradients in the troposphere. The aircraft sites are located mainly over the North American continent but also include some sites over the Pacific Ocean (Figure 1). The aircraft profiles also include measurements over the Southern Great Plains (SGP), operated by the U.S. Department of Energy [*Biraud et al*., 2013]. Most of the aircraft profiles range between the surface and 350 hPa. For shorter periods, flights up to 150 hPa are available for the sites Charleston, South Carolina (SCA), SGP, and Cartersville, Georgia (VAA), also covering the UTLS (upper troposphere/lower stratosphere) region.

[11] In addition, we compare model simulations with CH_4 measurements from the HIAPER Pole-to-Pole Observations (HIPPO) program (http://hippo.ornl.gov/) [*Wofsy*, 2011]. We use the HIPPO-1 to HIPPO-3 campaigns, which were performed in January 2009 (HIPPO-1), October/November 2009 (HIPPO-2), and March/April 2010 (HIPPO-3). HIPPO measurements were mostly performed over the Pacific (but also partly cover the North American continent) between 82°N and 67°S (Figure 1), with continuous profiling between approximately 150 m and 8500 m altitudes, but also including many profiles of up to 14 km altitude. The HIPPO CH_4 measurements have been made in situ at high frequency using a quantum cascade laser spectrometer (QCLS) [*Kort et al*., 2011, 2012]. Furthermore, air samples were collected using

Table 1. Emission Inventories Used as A Priori[a]

Source Category	Reference	IAV	Emissions (Tg CH_4/yr)	Remarks
Wetlands				
Wetlands	"JK" inventory [*Bergamaschi et al*., 2007]	CLIM	174.9	[b]
Wetlands	LPJ WHyMe [*Spahni et al*., 2011]	2000–2008	137.6–153.2	[cd]
Rice				
Rice	EDGARv4.2	2000–2008	32.4–37.5	[ef]
Biomass Burning				
Biomass burning	GFEDv3.1 [*van der Werf et al*., 2010]	2000–2010	12.7–23.3	
Remaining Sources				
Coal mining	EDGARv4.2	2000–2008	27.9–46.7	[e]
Oil production, transmission, and handling	EDGARv4.2	2000–2008	15.8–16.9	[e]
Gas production and transmission	EDGARv4.2	2000–2008	41.2–52.1	[e]
Enteric fermentation	EDGARv4.2	2000–2008	91.3–100.2	[e]
Animal waste management	EDGARv4.2	2000–2008	10.8–11.5	[e]
Waste handling	EDGARv4.2	2000–2008	54.5–60.6	[e]
Other anthropogenic sources	EDGARv4.2	2000–2008	18.7–21.1	[eg]
Wild animals	*Houweling et al*. [1999]	CLIM	5.0	
Termites	*Sanderson* [1996]	CLIM	19.3	
Ocean	*Lambert and Schmidt* [1993]	CLIM	17.0	
Soil sink	*Ridgwell et al*. [1999]	CLIM	−37.9	

[a]The third column ("IAV") indicates the available time period of interannually varying emissions inventories (within the period 2000–2010). "CLIM" denotes climatology (i.e., the same emissions were applied for all years). The fourth column gives the total annual emissions (in Tg CH_4/yr; in case of interannually varying emissions, it is the range of total annual emissions).
[b]Original inventory scaled to 175 Tg CH_4/yr; 3 month running mean applied.
[c]Including categories "peatland," "wetlands," and "wet soils" of *Spahni et al*. [2011], using their original inventories based on the LPJ WHyMe dynamic global vegetation model (DGVM) v1.3.1 model without applying their recommended scaling factors (based on their atmospheric inversions).
[d]For 2009 and 2010, the average emissions from 1990 to 2008 were applied (S2-SCIA and S2-NOAA).
[e]For 2009 and 2010, the EDGARv4.2 emissions from 2008 were applied as a priori (all inversions except S3-SCIA and S3-NOAA).
[f]Applying the seasonal distribution from *Matthews et al*. [1991].
[g]Including CH_4 emissions from use of fossil fuels and biofuels, energy manufacturing transformation, fossil fuel fires, industrial processes and product use and agricultural waste burning.

the NOAA Programmable Flask Package and analyzed at NOAA ESRL. Comparison of the QCLS measurements (10 s average) with NOAA flask samples taken within the same 10 s time interval showed a small bias of 3.5 ppb for HIPPO-1, 3.9 ppb for HIPPO-2, and 6.0 ppb for HIPPO-3 (QCLS-NOAA discrete samples; median of the differences of all simultaneous measurements). In this study, we subtract this bias from the QCLS measurements.

[12] Further aircraft measurements were provided by the CARIBIC (Civil Aircraft for the Regular Investigation of the atmosphere Based on an Instrument Container) program using a Lufthansa A340-600 passenger aircraft [*Brenninkmeijer et al*., 2007; *Schuck et al*., 2010, 2012]. The CARIBIC flights start from Frankfurt (Germany) to various destinations in North and South America, South Africa, and Asia (Figure 1), with typically two to four flights per month (starting in May 2005). Twenty-eight samples were collected at cruise altitude for most months. CH_4 mixing ratios were analyzed in the Max Planck Institute (MPI) Mainz laboratory, calibrated against the NOAA2004 scale.

[13] Finally, we use measurements from the BARCA (Balanço Atmosférico Regional de Carbono na Amazônia) aircraft campaigns over the Amazon, performed in November 2008 (BARCA-A) and May 2009 (BARCA-B) [*Beck et al*., 2012]. During both campaigns, flask samples were collected, which were subsequently analyzed for CH_4 in the MPI Jena laboratory. During BARCA-B, CH_4 mixing ratios were also measured in situ, using cavity ring-down spectroscopy [*Chen et al*., 2010]. Both flask and in situ measurements are calibrated against the NOAA2004 scale. For model validation in this study, we use a merged data set of the BARCA-B flask and in situ measurements, averaging all available measurements within 30 min in a given vertical layer.

3. Modeling

3.1. TM5-4DVAR Inverse Modeling System

[14] We use the four-dimensional variational (4DVAR) inverse modeling system TM5-4DVAR described in detail by *Meirink et al*. [2008] including subsequent further developments described by *Bergamaschi et al*. [2009, 2010]. The set of model parameters (state vector $\boldsymbol{x}$) is optimized by iteratively minimizing the cost function:

$$J(\boldsymbol{x}) = \frac{1}{2}(\boldsymbol{x}-\boldsymbol{x}_B)^{\mathrm{T}}\mathbf{B}^{-1}(\boldsymbol{x}-\boldsymbol{x}_B) + \frac{1}{2}\sum_{i=1}^{n}(H_i(\boldsymbol{x})-\boldsymbol{y}_i)^{\mathrm{T}}\mathbf{R}_i^{-1}(H_i(\boldsymbol{x})-\boldsymbol{y}_i), \quad (1)$$

where $\boldsymbol{x}_B$ is the a priori estimate of $\boldsymbol{x}$, $\mathbf{B}$ the parameter error covariance matrix, $\boldsymbol{y}$ the set of observational data, $\mathbf{R}$ the observation error covariance matrix, and $H(\boldsymbol{x})$ the model simulations corresponding to the observations. The state vector includes the emissions per model grid cell, month, and emission group, the initial 3-D CH_4 fields at the beginning of each inversion series, and the parameters for the bias correction of the SCIAMACHY retrievals (see section 3.2). We apply a "semiexponential" description of the probability density function for the a priori emissions to force the a posteriori emissions to remain positive [*Bergamaschi et al*., 2009, 2010]. The cost function equation (1) is minimized by evaluating its gradient with respect to the state vector using the adjoint of the tangent linear model

Table 2. Settings of Different Inversions (See Section 3.2 for Further Details)

Inversion	Observations	Bias Correction	A Priori Inventories	OH	Period
S1-SCIA	SCIAMACHY + NOAA	polynomial	EDGARv4.2/JK[a]	TM5[d]	2003–2010
S2-SCIA	SCIAMACHY + NOAA	polynomial	EDGARv4.2/WHyMe[b]	TM5[d]	2003–2010
S3-SCIA	SCIAMACHY + NOAA	polynomial	EDGARv4.2-CONST[c]/JK[a]	TM5[d]	2003–2010
S4-SCIA	SCIAMACHY + NOAA	polynomial	EDGARv4.2/JK[a]	SP[e]	2003–2010
S5-SCIA	SCIAMACHY + NOAA	smooth	EDGARv4.2/JK[a]	TM5[d]	2003–2010
S1-NOAA	NOAA only		EDGARv4.2/JK[a]	TM5[d]	2000–2010
S2-NOAA	NOAA only		EDGARv4.2/WHyMe[b]	TM5[d]	2000–2010
S3-NOAA	NOAA only		EDGARv4.2-CONST[c]/JK[a]	TM5[d]	2000–2010
S4-NOAA	NOAA only		EDGARv4.2/JK[a]	SP[e]	2000–2010

[a]Wetland inventory of J. O. Kaplan [*Bergamaschi et al*., 2007].
[b]LPJ WHyMe inventory [*Spahni et al*., 2011].
[c]Using the same anthropogenic emissions for all years (EDGARv4.2 inventory for 2005; for biomass burning, the GFEDv3.1 average over the period 1997–2010 is used).
[d]OH fields from a TM5 full chemistry run.
[e]OH fields from *Spivakovsky et al*. [2000].

operator [*Bergamaschi et al*., 2010; *Krol et al*., 2008; *Meirink et al*., 2008] and employing the m1qn3 algorithm for minimization [*Gilbert and Lemaréchal*, 1989].

[15] The 4DVAR system is based on the off-line transport model TM5 [*Krol et al*., 2005], driven by meteorological fields from the European Centre for Medium-Range Weather Forecasts (ECMWF) ERA-Interim reanalysis [*Dee et al*., 2011]. We employ the standard TM5 version (TM5 cycle 1), with 25 vertical layers, and apply a horizontal resolution of $6° \times 4°$.

3.2. Inversion Setup

[16] The emission inventories used as a priori estimates are compiled in Table 1. In the inversion, four groups of emissions are optimized independently: (1) wetlands, (2) rice, (3) biomass burning, and (4) all remaining source categories [*Bergamaschi et al*., 2010]. This approach aims to separate these four emission groups based on their different spatial distributions and seasonal variations. We assume an uncertainty of 100% of a priori emissions (per $6° \times 4°$ TM5 model grid cell and month) for the first three emission groups and 50% for the "remaining sources." The temporal error correlations for the first three emission groups, which all exhibit large seasonal cycles, are set to zero, thus allowing maximum flexibility to optimize the a priori seasonal variation. The temporal correlation for the "remaining sources," which are assumed to be relatively constant throughout the year, is set to 9.5 months to suppress large seasonal variations in the a posteriori emissions of this emission group. Spatial error correlations of 500 km are adopted for all four emission groups. Single SCIAMACHY measurements are averaged over a $1° \times 1°$ grid and over the length of the individual assimilation time slots (set to 3 h). The assigned uncertainties include the statistical fit error of the individual SCIAMACHY pixels, the standard deviation of the pixels within $1° \times 1°/3$ h, and potential additional errors (set to 1%) [*Bergamaschi et al*., 2009]. For the surface observations, we assume a measurement uncertainty of 3 ppb but take into account also the model representation error, depending on local emissions and 3-D gradients of simulated CH_4 mixing ratios [*Bergamaschi et al*., 2010], resulting in an average total uncertainty of ~10 ppb for the surface data (ranging between 3 ppb and more than 100 ppb). Chemical destruction of CH_4 by OH radicals in the troposphere is simulated using either (1) OH fields from a TM5 full chemistry run based on Carbon Bond Mechanism 4, optimized based on methyl chloroform (MCF) measurements [*Bergamaschi et al*., 2009, 2010], or alternatively (2) OH fields from *Spivakovsky et al*. [2000], adopting the recommended MCF-based scaling factor of 0.92 [*Huijnen et al*., 2010; *Patra et al*., 2011]. Both (scaled) OH fields result in virtually identical CH_4 lifetimes of 10.1 years (total CH_4 versus tropospheric OH).

[17] Chemical destruction of CH_4 by OH, Cl, and $O(^1D)$ in the stratosphere is based on the 5th generation European Centre Hamburg general circulation model (ECHAM5) Modular Earth Submodel System version 1 (MESSy1) [*Jöckel et al*., 2006], using the average sinks during 1999–2002. All photochemical sinks applied in this study are considered to be climatological; i.e., they do not take into account interannual variability (see also discussion in section 4.3).

[18] The inversions over the whole target period (2000–2010 for the inversions based on NOAA surface observations only and 2003–2010 for the combined SCIAMACHY + NOAA inversions) are split for technical reasons (the number of required iterations grows with length of the inversion window) into blocks of 18 months (first block 19 months), with an overlap of 6 months between consecutive blocks. While in the first 19 month inversion the initial field is (slightly) optimized further, each consecutive inversion is starting with the optimized 3-D fields of the previous inversion at 01 January (and the last 6 months of the previous inversion are discarded and not further used in the analysis). This approach ensures (1) that emissions are generally constrained by all observations at least 6 months after emission and (2) that the total CH_4 budget is closed in the model over the whole time series (i.e., the increase in the global burden is equal to total emissions minus total sinks over the whole target period).

[19] We performed nine different inversions, as compiled in Table 2: These include five inversions based on the simultaneous use of NOAA surface and SCIAMACHY observations (denoted Sx-SCIA) and four inversions using only NOAA surface observations (Sx-NOAA). Furthermore, the respective inversions use different a priori emission inventories, different tropospheric OH fields, and different bias corrections for the combined SCIAMACHY + NOAA inversions. Compared to the two "reference inversions" S1-SCIA and S1-NOAA, the inversions S2-SCIA and S2-NOAA explore the impact of using the (interannually varying) Lund-Potsdam-Jena dynamic global vegetation model with Wetland Hydrology

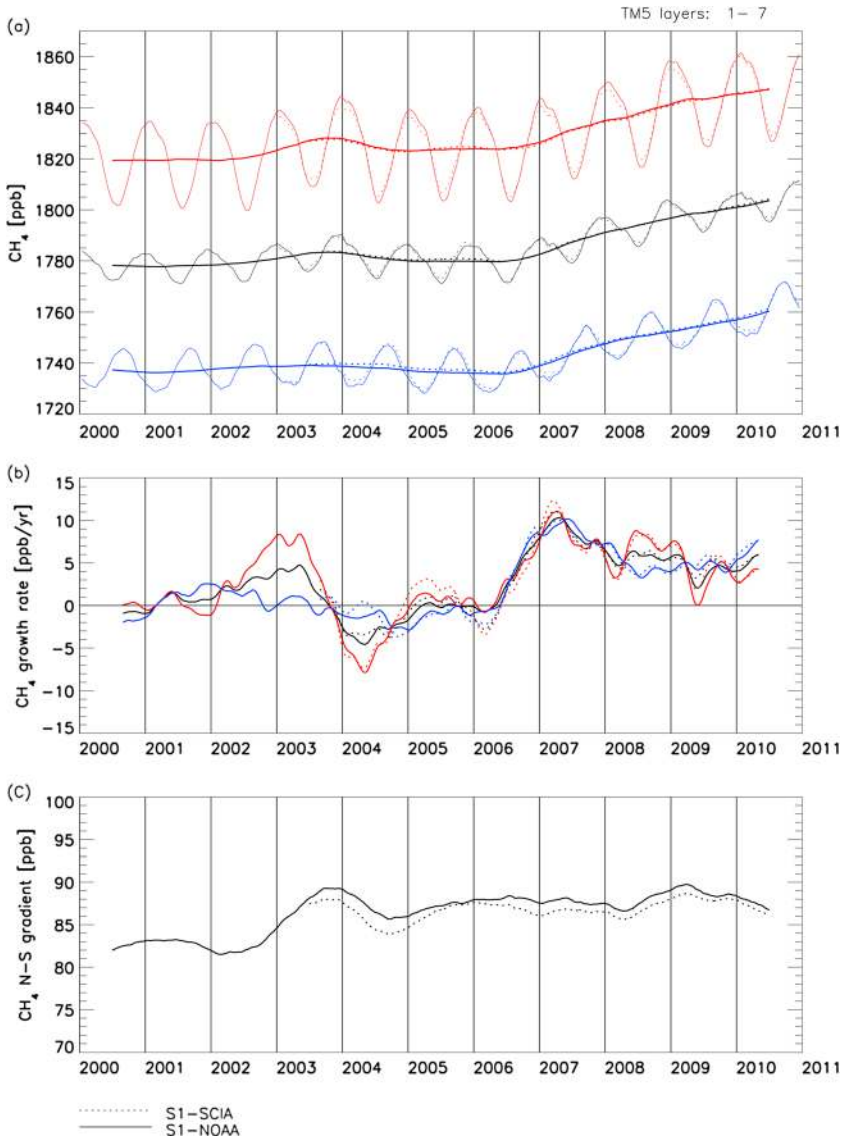

Figure 2. (a) Global and hemispheric mean CH_4 mixing ratios (black: globe; red: NH; blue: SH), evaluated for the seven lowest model layers (i.e., between the surface and ~2 km altitude); shown for S1-SCIA (dotted curve) and S1-NOAA (solid curve). The thick curve shows deseasonalized (12 month running mean) values. (b) Growth rate of global and hemispheric mean CH_4 mixing ratios. (c) Interhemispheric CH_4 gradient.

and Methane (LPJ WHyMe) inventory [*Spahni et al*., 2011], instead of the climatological inventory of J. O. Kaplan [*Bergamaschi et al*., 2007], as a priori for wetland emissions. In S3-SCIA/NOAA, the same a priori inventories are applied for each year, using the EDGARv4.2 inventory for 2005 for anthropogenic emissions and the Global Fire Emissions Database version 3.1 (GFEDv3.1) average over the period 1997–2010 for biomass burning. The objective of the S3-SCIA/NOAA inversions is to explore IAV derived in the inversion in the absence of a priori IAV. In S4-SCIA/NOAA, the TM5 OH fields are replaced by the OH fields from *Spivakovsky et al*. [2000]. The SCIAMACHY + NOAA inversions (S1-SCIA) - (S4-SCIA) apply a polynomial bias correction (second-order polynomial as a function of latitude and month [*Bergamaschi et al*., 2009]), while in S5-SCIA, a novel, "smooth" bias correction is applied, to allow a more flexible correction of the latitudinal bias component. The "smooth" bias uses one bias parameter per 1° latitude and month, taking into account a latitudinal correlation of the bias correction, which has been set to 10° latitude in S5-SCIA. For both approaches, the bias correction is constrained by the surface observations, especially those in the remote atmosphere, which measure the latitudinal gradient of the background atmosphere with high accuracy and hence serve as anchor points for the bias correction.

[20] Table S2 and Figure S1 summarize the statistics of the different inversions, demonstrating the excellent performance of the assimilation with an average bias (difference between model simulations and observations) close to zero for both the station and satellite data. Furthermore, this

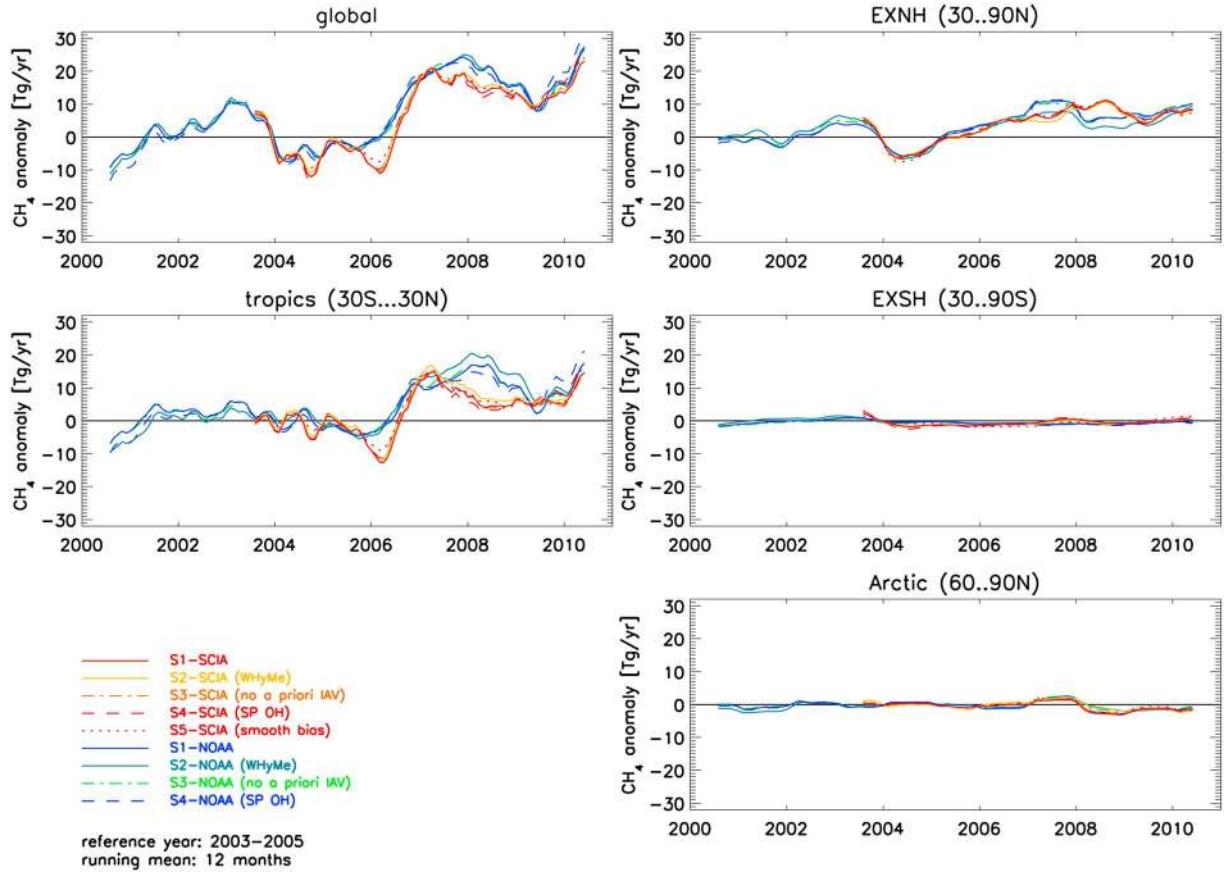

Figure 3. Interannual variation of total CH_4 emissions derived from the different inversions. The variations are shown relative to the average emissions during the reference period 2003–2005 (12 month running mean values).

compilation shows that the fit of the station data is only marginally degraded when including the satellite data (increase in root-mean-square (RMS) by 0.1–0.4 ppb for Sx-SCIA compared to corresponding Sx-NOAA).

4. Results and Discussion

4.1. Atmospheric CH_4 Mixing Ratios

[21] Modeled global and hemispheric average CH_4 mixing ratios are shown in Figure 2a, averaged over the seven lowest model layers (i.e., between the surface and ~2 km altitude, shown for S1-SCIA and S1-NOAA). The growth rate (Figure 2b) is calculated from the slope of the deseasonalized average mixing ratios. The figure illustrates the pronounced increase of the CH_4 growth rate in 2006, almost simultaneously in both hemispheres, peaking at ~10 ppb/yr in early 2007, followed by a slow attenuation.

[22] A different CH_4 anomaly is apparent during 2002–2004, being mostly in the Northern Hemisphere (NH), while the CH_4 mixing ratios in the Southern Hemisphere (SH) remain stable during the entire period 2000–2005. This 2002–2004 anomaly is therefore clearly visible in the interhemispheric gradient (Figure 2c), increasing by ~8 ppb between 2002 and late 2003, reflecting the increasing CH_4 mixing ratios in the NH during this period. In 2004, the CH_4 mixing ratios in the NH show a significant negative anomaly (negative growth rate), leading again to a reduction of the interhemispheric gradient. Between the beginning of 2005 and mid-2010, the interhemispheric gradient remains relatively stable, also during 2006–2007, consistent with the earlier observation that the CH_4 increase during this period occurs almost simultaneously in both hemispheres (as was also reported by *Rigby et al.* [2008], based on the Advanced Global Atmospheric Gases Experiment (AGAGE) and the Australian Commonwealth Scientific and Industrial Research Organisation (CSIRO) networks).

[23] The global and hemispheric average CH_4 mixing ratios in the lower atmosphere and the growth rates calculated from 3-D model fields are very robust, showing, in general, only weak dependence on the inversion settings. This also holds for the evolution of CH_4 growth rates at the latitudinal resolution of the transport model (4° latitude), shown in Figure S2 for all sensitivity experiments.

[24] We note, however, some differences in the mean CH_4 mixing ratios evaluated from the 3-D model fields compared to the NOAA CH_4 Marine Boundary Layer (MBL) Reference (http://www.esrl.noaa.gov/gmd/ccgg/mbl/; see Figure S3). The latter is, on average, ~5 ppb lower and shows a somewhat different seasonal cycle than the mean CH_4 mixing ratios evaluated from the 3-D model fields. While the model simulates the NOAA surface observations, in

Table 3. Change of Derived Average Emissions for 2007–2010 Compared to the Average for 2003–2005 for All Inversion Experiments (Tg CH_4/yr)

	90°N–60°N	60°N–30°N	30°N–EQ	EQ–30°S	30°S–60°S	60°S–90°S	Total
S1-SCIA	−1.0	8.3	10.1	−0.9	−0.1	0.0	16.3
S2-SCIA	−0.7	7.5	11.2	−0.9	−0.3	0.0	16.8
S3-SCIA	−0.8	8.4	9.5	−0.8	0.0	0.0	16.4
S4-SCIA	−0.9	8.4	10.3	−0.9	0.0	0.0	16.8
S5-SCIA	−0.5	7.9	8.5	1.3	−0.1	0.0	17.0
S1-NOAA	−0.8	9.1	6.7	5.6	−0.8	0.0	19.7
S2-NOAA	−0.6	6.6	10.0	4.5	−0.7	0.0	19.8
S3-NOAA	−0.3	8.4	6.7	5.7	−0.7	0.0	19.8
S4-NOAA	−0.8	9.0	7.1	5.8	−1.1	0.0	20.0

general, quite well (see Figure S4), these differences are mainly due to the fact that the integration of model fields over the whole model domain includes the continental air masses. Integrating the model fields only over the MBL results in mean CH_4 mixing ratios much closer to the NOAA MBL Reference method (see Figure S3). The remaining differences, especially in the NH seasonality, probably indicate a somewhat better representation of mean mixing ratios in the 3-D model fields, because they have complete spatial coverage of the MBL that is constrained by the actual, but more limited, observations.

4.2. Derived Total Emissions

[25] Figure 3 gives an overview of the interannual variability of total emissions derived from all inversion experiments. The derived global total emissions rose significantly between early 2006 and late 2008, and the average emissions during 2007–2010 are 16–20 Tg CH_4/yr higher than those during the period 2003–2005 (Table 3). This increase is mainly attributed to the tropics (with an increase of 9–14 Tg CH_4/yr for the average emissions for 2007–2010 compared to the average for 2003–2005) and the extratropical NH (increase of 6–8 Tg CH_4/yr). Further separation of derived emissions into 30° latitude bands shows that the latter increase is almost entirely attributed to the NH midlatitudes (between 30°N and 60°N; Figure S5a and Table 3), while the Arctic latitudes show only very small differences between these two periods (decrease by 0.3–1.0 Tg CH_4/yr). Clearly visible is significant IAV of global emissions during 2002–2004, largely attributed to the extratropical NH, consistent with the observation of the interannual variations of the CH_4 growth rate in the NH during that period (see section 4.1).

[26] While the global trends and IAV patterns are broadly consistent among all nine inversion experiments, differences are apparent between inversions using SCIAMACHY + NOAA data and those using only NOAA surface data, mainly for the tropics. The SCIAMACHY + NOAA-based inversions show a small negative anomaly during the first half of 2006 and a less pronounced positive anomaly between the end of 2007 and the beginning of 2009 (compared to the NOAA-only inversions). These differences in the tropical emission anomalies largely determine the differences visible in the emission anomalies of the global totals (Figure 3). Figure S5a shows that the differences in the tropical anomalies are somewhat larger in the NH tropics compared to the SH tropics. Furthermore, we see some differences between the SCIAMACHY + NOAA and NOAA-only inversions for the midlatitudes of the NH during 2007–2008, while the Arctic shows very high consistency among all scenarios during the entire target period (we note, however, that Arctic latitudes are not directly constrained by SCIAMACHY in our inversions). In Figure S7a, we also present zonal emission anomalies at the latitudinal resolution of the model (4° latitude), revealing significant differences in the "latitudinal fine structure" of the emission anomalies between the SCIAMACHY + NOAA-based inversions and the NOAA-only inversions. In general, however, this fine structure is very similar for the inversions (S1-SCIA) - (S4-SCIA) demonstrating that these inversions are strongly constrained by the SCIAMACHY observations (in addition to NOAA surface data), while inversions (S1-NOAA) - (S4-NOAA) show a somewhat stronger sensitivity to the inversion settings.

[27] Significant differences in the latitudinal fine structure between the SCIAMACHY + NOAA and the NOAA-only inversions were expected since the satellite data provide significant additional constraints especially for tropical regions. Yet the central challenge remains to evaluate the quality of the additional information from the satellite data and to identify potential artifacts. For example, the negative anomaly derived for tropical regions during the first half of 2006 for the SCIAMACHY + NOAA inversions is very likely directly related to the negative tropical anomaly visible in the deseasonalized time series of the SCIAMACHY retrievals [see *Frankenberg et al*., 2011, Figure 7]. At the same time, however, the SCIAMACHY retrievals over Africa show a larger anomaly than that observed by NOAA at Assekrem, Algeria [see *Frankenberg et al*., 2011, Figure 10], during that period. It is currently not clear if the inconsistency of the time series during that period is due to the limited region of influence for air samples collected at Assekrem or due to a potential artifact in the SCIAMACHY retrievals caused by the detector degradation which occurred late 2005.

[28] Also, the bias correction of the SCIAMACHY retrievals plays a significant role. While the previous IMAPv5.0 retrievals [*Frankenberg et al*., 2008], available for 2003–2005, showed only a very small latitudinal bias component [*Bergamaschi et al*., 2009], the extension of the SCIAMACHY retrievals beyond the end of 2005 required the application of a consistent (but more strict) pixel mask over the entire period 2003–2010 (IMAPv5.5 retrievals used in this study), which reintroduced a strong latitudinal dependence of the bias [*Frankenberg et al*., 2011], making the inversions more sensitive to the applied bias correction. While, in inversions (S1-SCIA) - (S4-SCIA) a polynomial bias correction as a function of latitude and month is applied, in S5-SCIA, we use a "smooth" bias correction (see section 3.2), which allows a more flexible compensation of potential biases

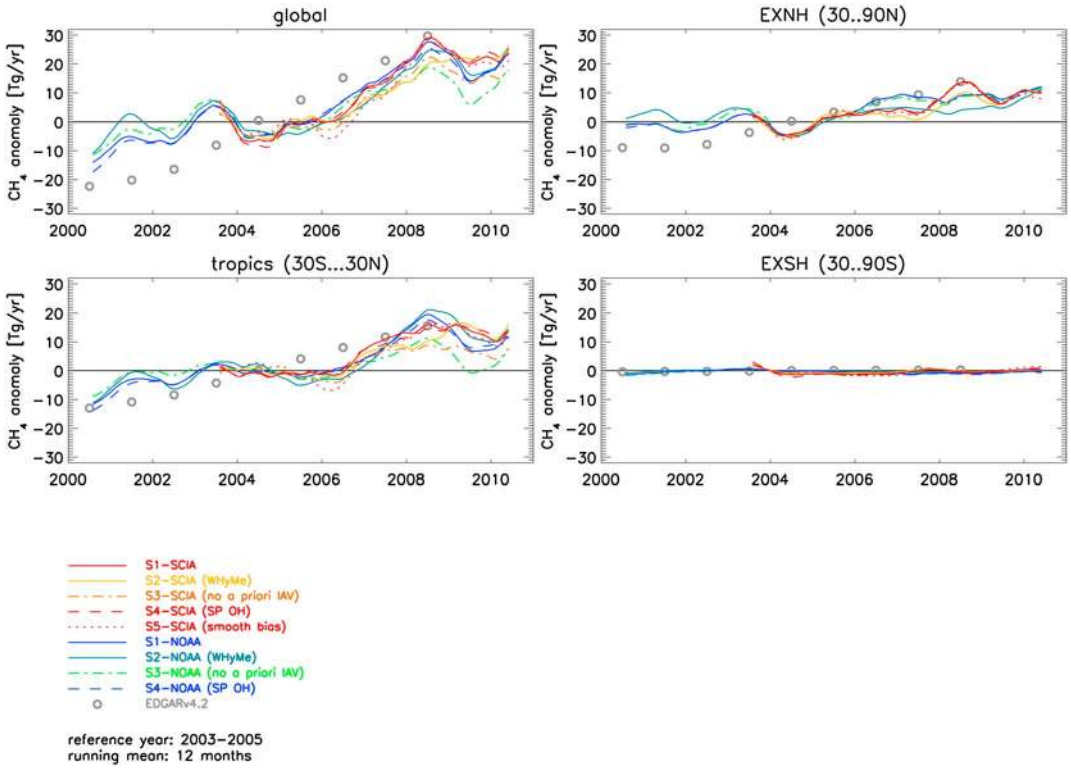

Figure 4a. (a) Interannual variation of anthropogenic CH_4 emissions (excluding biomass burning) derived from the different inversions. These include the anthropogenic sources listed in Table 1 under "remaining sources" (i.e., excluding the minor natural sources and sinks) and rice emissions. In addition, the interannual variation of the corresponding anthropogenic emissions from the EDGARv4.2 inventory during 2000–2008 is shown, applied to all scenarios as a priori (for 2009–2010, the EDGARv4.2 emissions for 2008 are used), except S3-SCIA/S3-NOAA, which use the same a priori anthropogenic emissions for all years.

on shorter latitudinal distances. The derived smooth bias correction shows indeed a significantly different latitudinal structure than the polynomial bias correction (Figure S10), and Figure S7a demonstrates a significant impact on the latitudinal fine structure of the derived emission anomalies in the tropics. Despite these differences, the emission anomalies derived from S5-SCIA are largely consistent with the emission anomalies derived from inversions (S1-SCIA) - (S4-SCIA) when averaged over 60° latitude bands (Figure 3) and, to a somewhat lesser extent, when averaged over 30° latitude bands (Figure S5a). In section 4.4, we will further evaluate the quality of the different sensitivity inversions using various independent validation data sets.

4.3. Attribution of Emission Anomalies to Major Source Categories

[29] Next, we analyze the attribution of interannual variations of total emissions to the major emission source categories.

4.3.1. Anthropogenic Emissions

[30] Comparing Figures 4a–4c shows that the increase of total emissions can be mostly attributed to the anthropogenic emissions (excluding biomass burning), with global anthropogenic emissions during 2007–2010 being 14–22 Tg CH_4/yr higher than the 2003–2005 average. Also, for S3-SCIA and S3-NOAA, in which constant emissions had been used as a priori, a significant increase of anthropogenic emissions is derived (14–16 Tg CH_4/yr higher emissions during 2007–2010 compared to 2003–2005), albeit somewhat smaller than that in the inversions guided by the EDGARv4.2 trend. This demonstrates that the inversion system can, to some extent, separate trends from different source categories with different spatial (and temporal) distributions.

[31] For all inversions, the derived overall trend of the anthropogenic emissions is smaller than the trend in the EDGARv4.2 emission inventory (shown as grey circles in Figure 4a). While the EDGARv4.2 emissions rise by 37.8 Tg CH_4/yr between 2003 and 2008 (which is the last year provided in EDGARv4.2), the inversions derive an increase of 12–26 Tg CH_4/yr during this period. Comparing the average for 2007–2008 with the 2003–2005 average, the EDGARv4.2 emissions increase by 25.4 Tg/yr, while the inversions yield only 15–22 Tg/yr higher emission. Between 2000 and 2008, the EDGARv4.2 emissions rise by 52.0 Tg CH_4/yr, with the average for 2007–2008 being 45.1 Tg CH_4/yr higher than the 2000–2002 average, compared to an increase of only 21–31 Tg CH_4/yr (2007–2008 versus 2000–2002 average) from the NOAA-only inversions (only the NOAA-only inversions include the period before 2003). Also, the temporal evolution shows significant differences: The EDGARv4.2 emissions increase steadily between 2000 and 2008, with an increased growth rate after 2002, while the inversions yield a large increase mostly since 2006. Anthropogenic CH_4 emissions have recently been reported also by *EPA* [2012] estimating an increase by

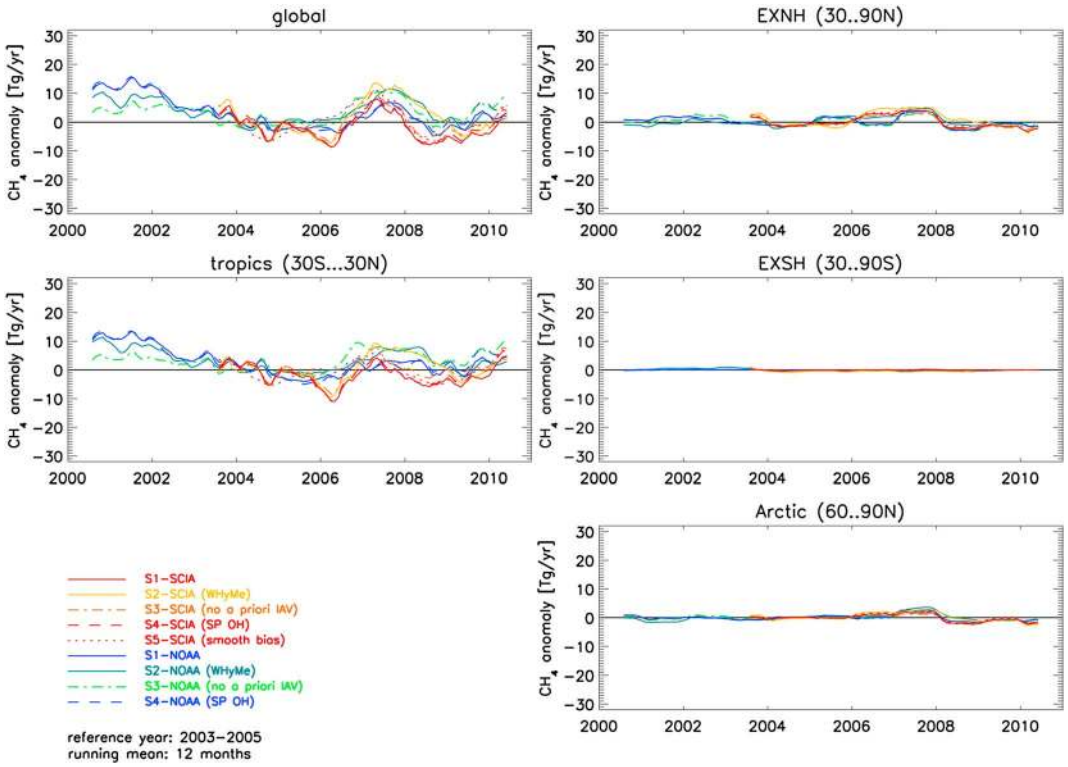

Figure 4b. Interannual variation of CH_4 emissions from wetlands derived from the different inversions. The variations are shown relative to the average emissions during the reference period 2003–2005 (12 month running mean values).

41.5 Tg CH_4/yr between 2000 and 2010, which is closer to the increase derived in the inversions than the EDGARv4.2 estimates. We note, however, that the *EPA* [2012] estimates for 2010 are projections based on a business-as-usual scenario.

[32] Most of the increase in anthropogenic emissions in the inversions is attributed to the tropics and extratropical NH (and within the latter, almost entirely to the midlatitudes between 30°N and 60°N; not shown). About half of the large increase of the global anthropogenic emissions in EDGARv4.2 is attributed to China, with an increase of 18.6 Tg CH_4/yr between 2003 and 2008, largely due to increased CH_4 emissions from coal mining (10.7 Tg CH_4/yr) and agriculture (increase by 4.9 Tg CH_4/yr from rice cultivation and enteric fermentation). The inversion also attributes a significant increase of anthropogenic CH_4 emissions to China (Figure 5), however at a much smaller rate: The inversions yield an increase of anthropogenic emissions of 1.1 ± 0.3 (0.4–1.4) Tg CH_4/yr per year (evaluated by using linear regression lines through the whole inversion period; Figure 5), equivalent to an increase of 5.4 ± 1.4 Tg CH_4/yr between 2003 and 2008. A significantly smaller increase of the Chinese anthropogenic emissions (compared to EDGARv4.2) is also estimated by *EPA* [2012] (increase by 7.3 Tg CH_4/yr between 2000 and 2010), mostly due to lower estimates of CH_4 emissions from coal mining.

[33] Substantial increases are also reported for other countries in EDGARv4.2; however, they were generally far smaller than that for China. The second largest increase of CH_4 emissions between 2003 and 2008 is reported for Brazil (+2.5 Tg CH_4/yr), followed by the Russian Federation (+2.0 Tg CH_4/yr) and India (+1.5 Tg CH_4/yr). A more detailed discussion of emission trends per country, however, is beyond the scope of this paper.

[34] SF_6 simulations performed within the framework of the TransCom-CH_4 initiative [*Patra et al*., 2011] showed that TM5 may underestimate interhemispheric mixing. This potential systematic transport error in TM5 may result in a low bias of the derived emissions for China. First experiments with an updated TM5 version, using a horizontal diffusion parameterization based on the scheme of *Prather et al*. [1987], improve the agreement between SF_6 simulations and observations and, applied in the inversion, lead to some latitudinal redistribution of derived total emissions while having only a negligible impact on the derived IAV of emissions (G. Monteil et al., Comparison of CH_4 inversions based on 15 months of GOSAT and SCIAMACHY observations, submitted to *Journal of Geophysical Research*, 2013).

[35] Besides the significant increasing trend of anthropogenic emissions, Figure 4a also shows the presence of considerable IAV. Some of this IAV may be an artifact due to imperfect separation of source categories in the inversion. Furthermore, IAV in the OH sink may also play some role (as discussed below).

4.3.2. Wetlands

[36] In Figures 4b and 4c, we show the derived IAV for wetlands and biomass burning, respectively, and in the supporting information, also the zonal emission anomalies at the latitudinal resolution of the model are presented (Figures S7b and S7c). A significant anomaly of wetland emissions is derived at Arctic latitudes during 2007 in all scenarios (1.2–3.2 Tg CH_4/yr), while subsequent years show slightly lower emissions (−1.6 to −0.9 Tg CH_4/yr) compared

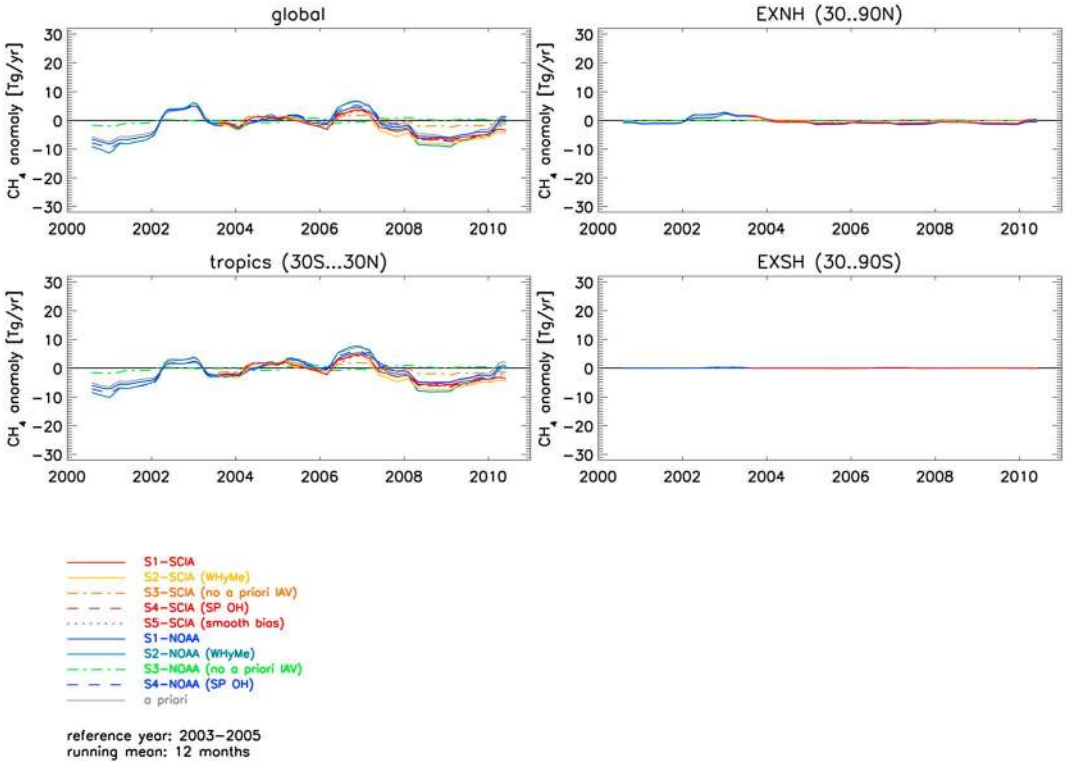

Figure 4c. Interannual variation of CH_4 emissions from biomass burning derived from the different inversions. In addition, the interannual variation from the GFEDv3.1 inventory is shown (applied to all scenarios as a priori, except S3-SCIA/S3-NOAA, which use the same a priori biomass burning emissions for all years). The variations are shown relative to the average emissions during the reference period 2003–2005 (12 month running mean values).

to the 2003–2005 average (between 60°N and 90°N). The positive anomaly visible in the total emissions in this region (Figure 3) is hence mostly attributed to wetlands, which are very likely the major driver of the observed CH_4 increase at high northern latitudes in 2007 (Figure S2). The enhanced Arctic wetland emissions in 2007 are very likely due to enhanced temperatures, especially over the Siberian Arctic [*Dlugokencky et al*., 2009; *Rigby et al*., 2008] (evaluated also in this study from ECMWF 2 m temperatures at model grid cells with wetland emissions; not shown). Although the absolute magnitude of the derived Arctic anomaly is relatively small, the effect on atmospheric CH_4 observed at the surface in this region is quite pronounced. This is due to the small surface area of the Arctic latitude band (60°N–90°N) representing only 13.4% of the hemispheric area. For comparison, the 30°N–60°N latitude band represents 36.6% and the tropical latitude (EQ–30°N) band 50% of the hemispheric area. Normalized by area, a 1 Tg CH_4/yr anomaly in the Arctic latitude band is equivalent to a 3.7 Tg CH_4/yr anomaly in the (EQ–30°N) latitude band or 7.5 Tg CH_4/yr in the whole tropical latitude band (30°S–30°N). Furthermore, the higher sensitivity of surface observations in the Arctic is amplified by the much less vigorous vertical mixing in the Arctic compared to the tropics [*Bousquet et al*., 2011].

[37] The derived IAV for wetlands in the tropics (30°S–30°N) ranges between −7 and +10 Tg CH_4/yr during 2003–2010 (compared to the 2003–2005 average; Figure 4b). These variations show, however, some differences among the different scenarios: During 2006, (S1-SCIA) - (S4-SCIA) show a significant negative anomaly (−3 to −7 Tg CH_4/yr) which is not visible in (S1-NOAA) - (S4-NOAA) (similar to the differences observed for the total tropical emissions; see Figure 3

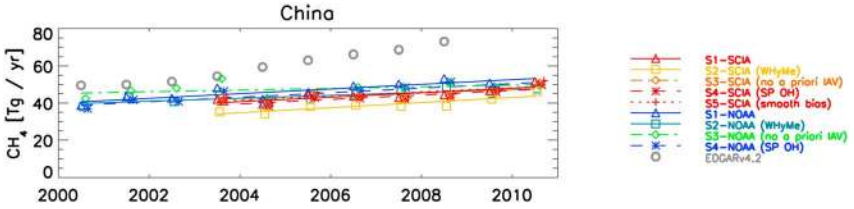

Figure 5. Anthropogenic emissions (except biomass burning) for China derived from the different inversions and from the EDGARv4.2 inventory (grey circles; applied to all scenarios as a priori, except S3-SCIA/S3-NOAA).

and section 4.2). Also, during 2007–2008, differences are apparent between the SCIAMACHY + NOAA and the NOAA-only inversions, and inversions using different a priori wetland inventories.

[38] Despite these differences, all inversions show a rather consistent increase of wetland emissions in the SH tropics (30°S–EQ) starting in 2006 and extending into 2007 (positive anomaly in 2007: 1–8 Tg CH_4/yr; see Figure S5b). This is very likely due to higher than average precipitation in the tropics [*Dlugokencky et al*., 2009] (evaluated also in this study from Global Precipitation Climatology Project version 2.2 (GPCPv2.2) precipitation at model grid cells with wetland emissions; not shown).

[39] The finding of increased wetland emissions in 2007 is qualitatively consistent with the inverse modeling study of *Bousquet et al*. [2011] (covering 2006–2008). However, they derived a much larger increase of wetland emissions between 2006 and 2007 (by 33 Tg CH_4/yr from their inversion INV1 [*Bousquet et al*., 2011, Table 3]), while in our study, the global wetland emissions in 2007 are only 5–12 Tg CH_4/yr higher compared to those in 2006. The significantly larger wetland anomaly in INV1 of *Bousquet et al*. [2011] is related to a larger anomaly of total emissions (increase by 31 Tg CH_4/yr between 2006 and 2007, compared to only 13–17 CH_4/yr in our study) and the fact that they attribute the increase in total emissions largely to wetlands (with an estimated decrease of 5 Tg CH_4/yr of anthropogenic sources), while in our study, a substantial fraction of the total increase is attributed to anthropogenic emission (5–12 Tg CH_4/yr).

[40] During 2000–2002, the NOAA-only inversions show higher global wetland emissions compared to the 2003–2005 average (2000–2002 average of 5–11 Tg CH_4/yr higher, mostly attributed to the tropics). While this positive anomaly is found also in S3-NOAA (using constant a priori emissions; 2000–2002 average of 5 Tg CH_4/yr higher), the significantly higher anomaly found in S1-NOAA, S2-NOAA, and S4-NOAA (8–11 Tg CH_4/yr) could be due to the overestimated increase of anthropogenic emissions in EDGARv4.2 (see above), which the inversion may compensate by attributing the required correction of total emissions partly also to wetlands.

4.3.3. Biomass Burning

[41] Although CH_4 emissions from biomass burning contribute only ~3–9% to total CH_4 emissions, they play a significant role for interannual variations of the global CH_4 budget during intensive fire events [e.g., *Bousquet et al*., 2006; *Langenfelds et al*., 2002]. According to the GFEDv3.1 inventory [*van der Werf et al*., 2010], CH_4 emissions from biomass burning vary between 12.7 and 23.3 Tg CH_4/yr during the period 2000–2010. Major anomalies during this period include the large fires in Indonesia in 2002 and 2006 and the large fires in boreal Asia in 2003 [*van der Werf et al*., 2010].

[42] In general, all inversions that use the GFEDv3.1 inventory as a priori (i.e., all inversions except S3-NOAA and S3-SCIA) follow largely the major patterns of IAV of this inventory (Figures 4c and S5c). Even at the latitudinal resolution of the model, a posteriori emissions from biomass burning are very consistent (Figures S6 and S7c). Remarkably, S3-SCIA (with constant a priori for all years) derives very similar IAV patterns between the equator and ~15°S (albeit with somewhat lower amplitude), while this is not the case for S3-NOAA. This illustrates the added value of the SCIAMACHY data and the capability of the inversion to derive realistic IAV patterns in regions with strong observational constraints. *Frankenberg et al*. [2011] pointed out that the XCH_4 retrievals based on the proxy method may have systematic errors in case of biomass burning plumes, if the coemitted CO_2 is not properly accounted for in the applied CO_2 correction. However, since the GFED inventory is applied as a priori in the ensemble Kalman filter CarbonTracker CO_2 inversion [*Peters et al*., 2007], the systematic error in the proxy retrievals should be small as long as the deviations from the GFED CO_2 emissions are small.

[43] According to GFEDv3.1, 8.6 Tg CH_4 was emitted in equatorial Asia during August–October 2006, compared to average emissions of 1.3 Tg CH_4 during the same 3 months in the period 2003–2005. These elevated emissions are due to the large Indonesian forest fires, peaking in October 2006, and are the major reason for the pronounced tropical (and global) anomaly visible in Figure 4c (see also Figures S5c and S7c). The Indonesian fires were related to drought during the 2006 El Niño and lead to significantly elevated CO and O_3 mixing ratios over Indonesia and the eastern Indian Ocean [*Logan et al*., 2008]. Elevated CH_4 mixing ratios over Indonesia in October 2006 have also been reported by *Worden et al*. [2013] based on measurements from the Aura Tropospheric Emission Sounder satellite instrument and were attributed to biomass burning using correlations between observed CH_4 and CO.

[44] Large forest fires also occurred in equatorial Asia in 2002 and in boreal Asia in 2002 and 2003, resulting in significantly elevated CH_4 emissions during these 2 years (Figures 4c, S5c, and S6). These emissions contributed significantly to the IAV of total CH_4 emissions (Figure 3). This finding is largely consistent with the analysis of *Simpson et al*. [2006], who concluded that anomalously high biomass burning is very likely a major driver of the atmospheric CH_4 anomaly in 2002/2003, based on parallel measurements of ethane and tetrachloroethene. Furthermore, a significant CO anomaly in the extratropical NH during 2002/2003 has been reported by *Yurganov et al*. [2005], attributed to the strong boreal fires, especially in Russia.

[45] Besides biomass burning, our inversions assign a significant positive anomaly also to anthropogenic CH_4 emissions (excluding biomass burning) in 2003, clearly visible in both the extratropical NH and the tropics (Figure 4a). However, biomass burning also affects OH, in particular due to the emitted CO (but also due to coemitted CH_4 and VOC). Since the IAV of OH is not taken into account in our inversion, any OH IAV will erroneously be projected to the derived IAV of emissions. Unfortunately, the IAV of OH is rather uncertain, and available studies provide a rather inconsistent picture. Based on methyl chloroform (MCF) measurements from nine remote atmospheric monitoring sites, *Montzka et al*. [2011] derived an IAV of global average OH concentrations ranging between −4% and +5% for the 12 month running mean during 2000–2007 compared to the 1998–2007 average. Their derived OH IAV includes a significant dip in late 2002 and low OH during 2006/2007, coinciding with the periods of elevated biomass burning. However, significantly lower OH IAV (maximum of ±2%) has been derived in the same study, based on a 3-D atmospheric chemistry transport model (CTM), which takes into account IAV of meteorology, photolysis rates, and biomass

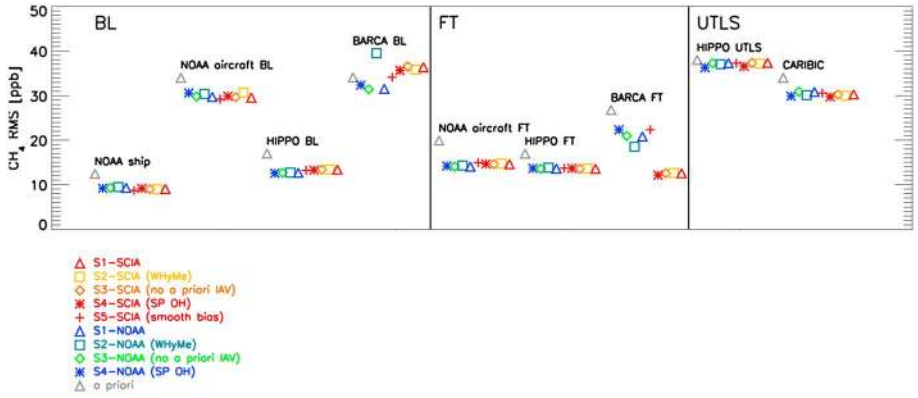

Figure 6. Model validation: RMS of differences between simulated CH_4 mixing ratios and independent observations in the boundary layer ("BL"), free troposphere ("FT"), and upper troposphere/lower stratosphere ("UTLS"). Observations are from NOAA shipboard samples, NOAA vertical profiles from light aircraft sampling, HIPPO and BARCA campaigns, and the CARIBIC program. "A priori" is from inversion S1 but starting from optimized 3-D fields at the beginning of each year (from inversion of the previous year; see section 3.2).

burning. Very low OH IAV was also derived by *Holmes et al*. [2013] using three independent CTMs. Furthermore, their results correlated poorly with the MCF-based OH IAV of *Montzka et al*. [2011]. Summarizing, despite the inconsistencies between the existing studies on OH IAV, it is obvious that OH IAV can play a significant role for the IAV of the global CH_4 budget, with an OH IAV of $\pm 1\%$ being equivalent to an IAV of the global sink of ± 5–6 Tg CH_4/yr. Further studies are required to better quantify OH IAV in which the coupling between the changes in CH_4 and CO needs to be considered involving their coupling with OH, as well as the impact of other relevant parameters (such as NO_x, water vapor, temperature, and stratospheric ozone).

4.4. Validation

[46] The quality of the model simulations is evaluated using various independent data sets of ship- and aircraft-based measurements, covering the boundary layer (BL), the free troposphere (FT), and the upper troposphere and lower stratosphere (UTLS) (see section 2.2 for description of the data sets and Figure 1). These additional observational data sets were not used in the inversions and therefore serve as independent validation of simulated 3-D CH_4 mixing ratios. Figure 6 gives an overview of the achieved root-mean-square (RMS) differences between model simulations and observations (using a total of ~104,000 measurements during 2003–2010). The figure illustrates the general significant improvement of optimized CH_4 mixing ratios from the inversions compared to the a priori simulations (shown for the a priori of inversion S1, which is, however, already partly optimized, since the a priori starts from optimized 3-D fields at the beginning of each year from the inversion of the previous year (see section 3.2)).

4.4.1. NOAA Ship Cruises

[47] Figure 7 shows the bias of model simulations (S1-SCIA) compared to NOAA samples from regular ship cruises through

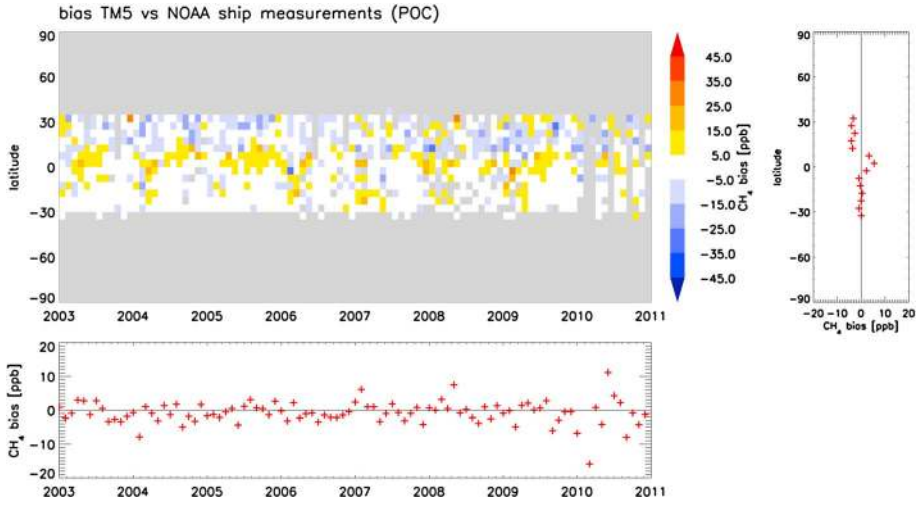

Figure 7. Validation of simulated CH_4 mixing ratios (S1-SCIA) using NOAA measurements on samples collected regularly on commercial ship lines through the Pacific Ocean (NOAA POC). Measurements and simulations are averaged in monthly 5° latitude bins. The bottom panel shows the monthly average over all latitudes. The panel on the right shows the average (per latitude bin) over the whole time period.

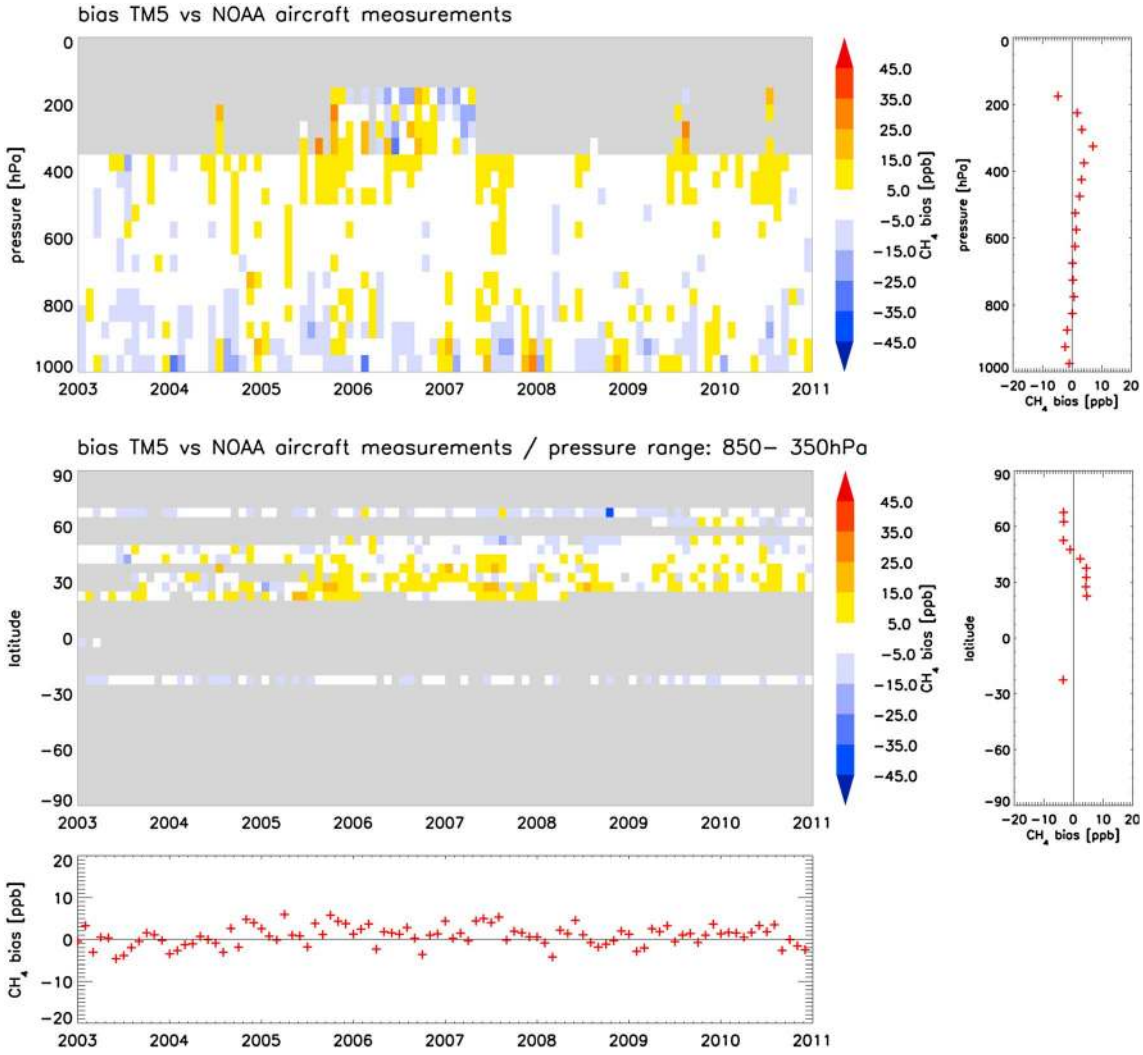

Figure 8. Validation of simulated CH_4 mixing ratios (S1-SCIA) using regular NOAA aircraft profiles (see also Figure 1 for the location of profiles). The top panel shows the bias as a function of altitude (pressure), and the middle panel shows the average bias in the FT as a function of latitude. The bottom panel shows the monthly average bias in the FT over all latitudes. The panels on the right show the average (per pressure/latitude bin) over the whole time period.

the Pacific Ocean (NOAA POC) as a function of time and latitude (averaged in monthly 5° latitude bins). The figure demonstrates the generally very good agreement, especially in the SH, where the bias is close to zero (76% of monthly 5° bins within 5 ppb; average bias over the whole 2003–2010 period < 1 ppb). A small negative bias is apparent in the NH (average bias ~ −3 to −4 ppb) and a small positive bias around the equator (maximum ~5 ppb). The figure also demonstrates the absence of any significant trends in the bias during the entire inversion period. The bias shows only minor differences among the different inversions (time series for the other inversions not shown), and the RMS values are very close for all inversions (~9 ppb; Figure 6).

4.4.2. NOAA Aircraft Profiles

[48] Compared to NOAA vertical profiles of CH_4, model simulations agree well in the free troposphere, with an average bias (averaged over 2003–2010) close to zero (Figure 8, top panel: bias as a function of altitude, averaged over all sites) and RMS values of 14–15 ppb for all inversions (Figure 6). Integrated over the free troposphere (defined here between 850 and 350 hPa), a small latitudinal dependence of the average bias is apparent (−3 to 4 ppb; Figure 8, middle panel).

[49] Within the boundary layer (between the surface and 850 hPa), the average bias is still very low (< 3 ppb; Figure 8, top panel); however, the RMS is significantly higher (~30 ppb) compared to that of the free troposphere and also compared to that of the NOAA ship measurements in the marine boundary layer. This is because many of the NOAA aircraft profiles are over the U.S. (see also Figure 1), close to regional CH_4 sources, which are not properly resolved by the coarse-resolution TM5 version used for the inversions.

[50] For shorter time periods (mainly between mid-2005 and beginning of 2007), NOAA profiles are available also for the upper troposphere (above 350 hPa) to the lower stratosphere (up to ~150 hPa/~13 km) for some of the aircraft sites.

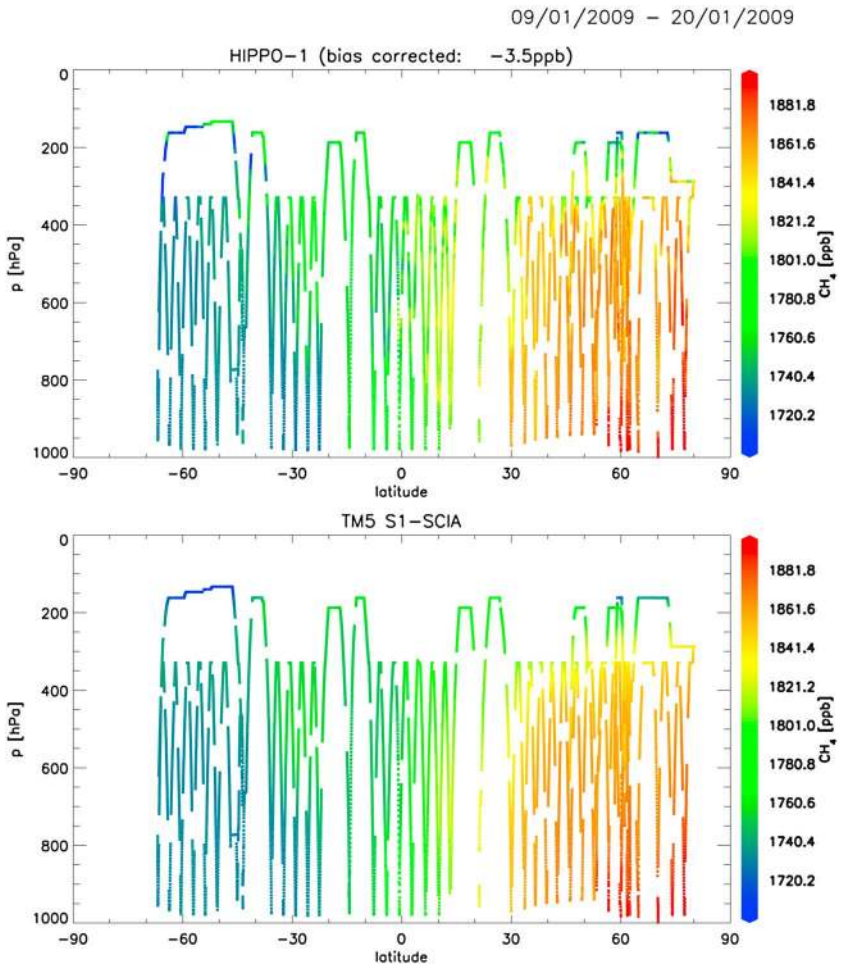

Figure 9. Validation using HIPPO aircraft data (HIPPO-1 southbound flight; S1-SCIA).

The monthly average bias (aggregated in 50 hPa bins) in this altitude region shows larger scatter compared to the free troposphere (Figure 8, top panel). This is partly attributed to the lower number of measurements in the UTLS compared to the free troposphere but is probably mainly due to the larger vertical gradients of CH_4 mixing ratios and occasional stratospheric intrusions into the upper troposphere, which are not resolved by the TM5 model.

4.4.3. HIPPO Aircraft Campaigns

[51] A very valuable data set for further validation is from the HIAPER Pole-to-Pole Observations (HIPPO) aircraft campaigns, providing transects from high northern (~80°N) to high southern latitudes (~70°S), between the surface and the UTLS. Figure 9 shows as example the southbound flight of HIPPO-1 (January 2009), demonstrating the overall very good agreement between observations and model simulations. Note that we applied a small correction to the HIPPO data (ranging between 3.5 and 6.0 ppb), determined by comparison with parallel discrete air samples, analyzed by NOAA ESRL (see section 2.2). Figure 10 shows the average bias (between TM5 and corrected HIPPO measurements) as a function of altitude, separated for the extratropical NH, tropics, and extratropical SH, for HIPPO-1 to HIPPO-3. Similar to the NOAA profiles, the bias is generally very low throughout the free troposphere. Furthermore, the bias varies only little between the different inversions (with a slightly smaller bias of S1-SCIA compared to S1-NOAA for HIPPO-1).

[52] There was also no significant bias between TM5 and HIPPO in the boundary layer, and the mean RMS for the boundary layer data from all HIPPO campaigns (~13 ppb) is very close to the HIPPO data in the free troposphere. The significant difference to the RMS from the NOAA aircraft data in the boundary layer (~30 ppb) reflects the fact that in contrast to the NOAA flights, the major part of the HIPPO transects is over the ocean.

[53] A significant deterioration of the bias is apparent above ~350 hPa for all three HIPPO campaigns, especially in extratropical regions. These deviations are attributed to the coarse horizontal ($6° \times 4°$) and vertical resolution (approximately five layers between 350 and 150 hPa) of the TM5 version used, which does not resolve, as mentioned before, the dynamics of stratospheric-tropospheric exchange on smaller scales.

4.4.4. CARIBIC Aircraft Measurements

[54] During the CARIBIC flights, especially in the extratropical NH, CH_4 mixing ratios up to ~100 ppb lower than model values are occasionally observed. The reason is that at middle to high latitudes given the cruise altitudes of 10–12 km, a significant fraction of the time is spent in the lowermost stratosphere. In Figure 11, we show the bias

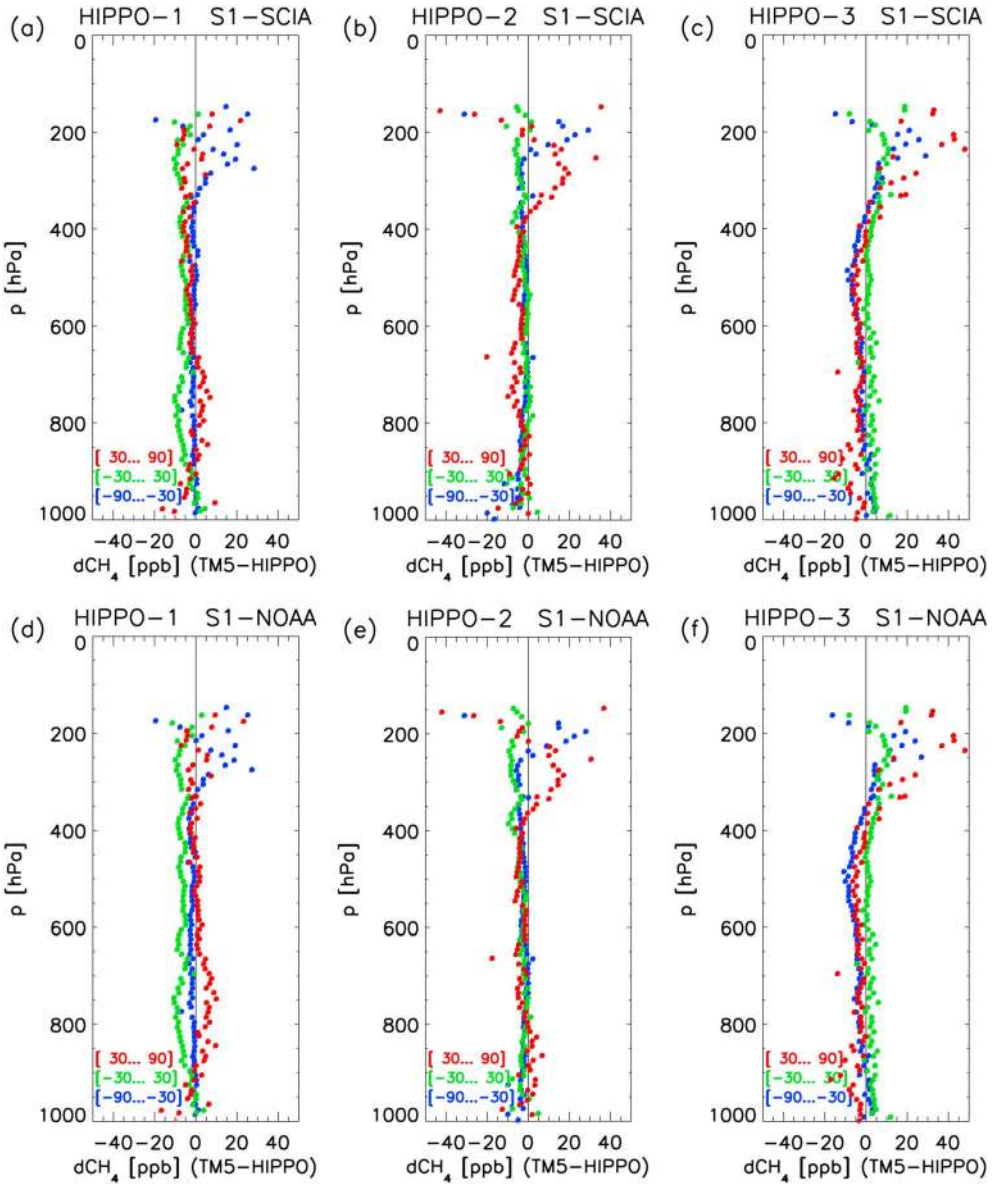

Figure 10. Validation using HIPPO-1 to HIPPO-3 aircraft data: average bias (TM5-HIPPO) as a function of altitude, separated for the extratropical NH (red), tropics (green), and extratropical SH (blue). (a–c) S1-SCIA; (d–f) S1-NOAA.

between TM5 and CARIBIC, after filtering data with clear stratospheric origin (based on potential vorticity), hence representing mainly the upper troposphere. While the monthly average bias still shows larger scatter as seen in the free troposphere (NOAA aircraft and HIPPO), the average bias between TM5 and CARIBIC over the whole period for which CARIBIC data exist (since August 2005) is very low (−6 to 3 ppb). Using the whole CARIBIC data set (i.e., without filtering for stratospheric influence), a RMS of 30–31 ppb is calculated, close to the RMS of the HIPPO data in the UTLS (36–37 ppb) (Figure 6).

4.4.5. BARCA Aircraft Campaigns

[55] Finally, we compare the model simulations with the BARCA aircraft campaigns over the Amazon. In contrast to the validation data sets discussed so far, the validation versus the BARCA data sets reveals significant differences among the inversions, with the RMS for (S1-SCIA) - (S4-SCIA) being significantly lower (12–13 ppb) compared to the corresponding inversions based on NOAA data only ((S1-NOAA) - (S4-NOAA) RMS: 19–22 ppb) in the free troposphere (Figure 6). While (S1-NOAA) - (S4-NOAA) result in lower CH_4 mixing ratios over the Amazon than observed during the BARCA flights (average bias in the FT: −19 to −14 ppb; Figures S8 and S9), (S1-SCIA) - (S4-SCIA) yield, on average, a much smaller bias (0 to 2 ppb). The tendency to underestimate CH_4 mixing ratios in the NOAA-only inversions is also clearly visible in the boundary layer, while the SCIAMACHY + NOAA-based inversions are too high in the boundary layer, especially for BARCA-B (Figure S9). The latter suggests that (S1-SCIA) - (S4-SCIA) may overestimate the regional emissions; however, given the coarse model resolution, the comparison with observations is more difficult to interpret (and much more

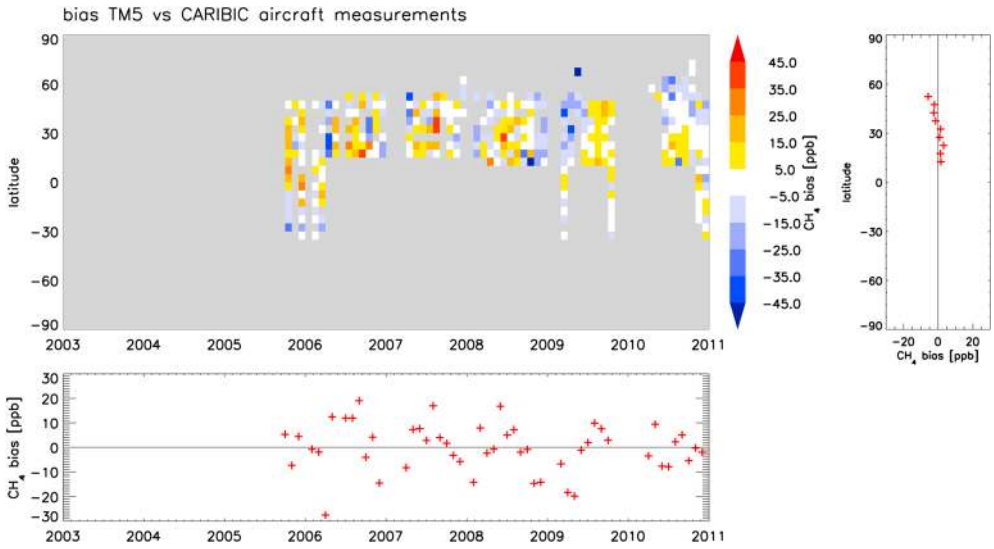

Figure 11. Validation of simulated CH_4 mixing ratios (S1-SCIA) using CARIBIC aircraft samples in the upper troposphere (see also Figure 1 for flight routes). Data with clear stratospheric origin were filtered out, based on potential vorticity (see text). Measurements and simulations are averaged in monthly 5° latitude bins. The bottom panel shows the monthly average over all latitudes. The panel on the right shows the average (per latitude bin) over the whole time period.

sensitive to model representation errors) in the boundary layer than in the free troposphere. S5-SCIA, which is using the smooth bias correction for the SCIAMACHY retrievals, results in mixing ratios that are too low (average bias: −20 ppb) and similar RMS as the NOAA-only inversions in the free troposphere. This finding indicates that the smooth bias correction may "overcorrect" the SCIAMACHY bias, assigning part of the emission signal to the bias correction.

[56] Summarizing, the comparison with the BARCA campaigns demonstrates the improvement of the inversions using both NOAA and SCIAMACHY data (S1-SCIA) - (S4-SCIA), using the polynomial bias correction), compared to the corresponding NOAA-only inversions in the free troposphere over the Amazon, consistent with the analysis of *Beck et al*. [2012] (which used, however, previous TM5-4DVAR inversions with somewhat different settings). We note, however, that this improvement does not necessarily imply that the derived IAV (which is the major focus of this paper) is more realistic in (S1-SCIA) - (S4-SCIA) compared to the NOAA-only inversions. While providing an important regional validation over the Amazon, these two intensive campaigns are not sufficient to draw clear conclusions about the differences in the IAV from the different inversions.

5. Conclusions

[57] This reanalysis of the global CH_4 cycle during the past decade suggests that global CH_4 emissions have increased significantly since 2006, with 16–20 Tg CH_4/yr higher emissions during 2007–2010 compared to the average emissions during 2003–2005. Most of this increase is attributed to the tropics and midlatitudes of the Northern Hemisphere, while no significant trend is derived for the Arctic latitudes. The increase in total CH_4 emissions is largely attributed to anthropogenic emissions. However, the derived trend in anthropogenic emissions (excluding biomass burning) is significantly lower compared to the trend in the EDGARv4.2 bottom-up emission inventory. Between 2003 and 2008, the EDGARv4.2 emissions rise by 37.8 Tg CH_4/yr, compared to only 12–26 Tg CH_4/yr derived from the inversions during this period. Comparing the average for 2007–2008 with the 2003–2005 average, the EDGARv4.2 emissions increase by 25.4 Tg/yr, while the inversions yield only 15–22 Tg/yr higher emission. About half of the large increase of global anthropogenic emissions in EDGARv4.2 is attributed to China, with an increase of 18.6 Tg CH_4/yr between 2003 and 2008, compared to an increase of only 5.4 ± 1.4 Tg CH_4/yr derived from the inversions.

[58] Superimposed on the increasing trend in anthropogenic CH_4 emissions are significant interannual variations of CH_4 emissions from wetlands (up to ± 10 Tg CH_4/yr) and biomass burning (up to ± 7 Tg CH_4/yr). A positive anomaly of wetland emissions (1–3 Tg CH_4/yr) has been derived for the Arctic in 2007, which is very likely the major driver for the large growth rate of atmospheric CH_4 observed at high northern latitudes in 2007. Furthermore, the inversions show a rather consistent increase of wetland emissions in the SH tropics (30°S–EQ), starting in 2006 and extending into 2007 (positive anomaly in 2007: 1–8 Tg CH_4/yr). Major biomass burning anomalies during 2000–2010 are related to the large fires in Indonesia in 2002 and 2006 and the large fires in boreal Asia in 2003. The IAV attributed to biomass burning in the inversions is probably largely driven by the applied a priori inventory (GFEDv3.1). However, inversion S3-SCIA (with constant a priori for all years) also derives very similar IAV patterns between the equator and ~15°S (albeit with lower amplitude), demonstrating the capability of the inversion to derive realistic IAV patterns in regions with strong constraints from satellite data. But, in general, the attribution to the different emission groups depends significantly on the applied a priori emission

inventories, while the derived IAV and trends for the total emissions are less sensitive to the a priori.

[59] Superimposed on the increasing trend, the inversions also attribute significant IAV to anthropogenic emissions. Although anthropogenic emissions may vary, in reality, more strongly than that suggested by the bottom-up inventory (EDGARv4.2) (e.g., due to potential climate dependence of agricultural emission), the IAV derived for anthropogenic emissions could be not only due to the mentioned limitations of the inversions to separate the different source categories but also due to IAV in OH, which was not considered in our study. Recent studies based on different atmospheric chemistry transport models estimated that the IAV of OH was relatively small during the last decade (maximum of ±2%) [*Holmes et al*., 2013; *Montzka et al*., 2011], while estimates based on MCF observations are somewhat higher (up to ~5%) [*Montzka et al*., 2011] and correlate poorly with the model-derived OH IAV patterns. Clearly, more studies are required to improve our understanding of OH IAV and to better disentangle IAV of CH_4 emissions and IAV of OH.

[60] While the above conclusions on derived emissions are largely consistent among all inversions, significant differences in the exact latitudinal attribution of the IAV of CH_4 emissions were apparent between the inversions using SCIAMACHY + NOAA data and those using only the NOAA surface observations. The differences are largest in the tropics, where the SCIAMACHY data provide strong constraints. The comparison with the BARCA aircraft campaigns (November 2008 and May 2009) clearly shows the significant improvement of the SCIAMACHY + NOAA inversions (S1-SCIA) - (S4-SCIA) compared to the NOAA-only inversions (S1-NOAA) - (S4-NOAA) in the free troposphere over the Amazon (albeit the (S1-SCIA) - (S4-SCIA) inversions overestimate CH_4 mixing ratios in the boundary layer). Despite this encouraging result that demonstrates the usefulness of the satellite data, one has to be cautious regarding conclusions about derived IAV, as potential artifacts in the SCIAMACHY retrievals cannot be ruled out, in particular, given the severe pixel degradation which occurred late 2005. The further shipboard and airborne validation data used in this study showed a generally very similar performance of all inversions (both in terms of RMS and bias). These observations are apparently too far away from the source regions in which the derived spatial emission distributions differ (mostly in the tropics). Comparison of model simulations with the NOAA ship and aircraft data showed very good agreement in the free troposphere and the remote marine boundary layer over the whole target period. Furthermore, validation against the HIPPO-1 to HIPPO-3 aircraft campaigns in 2009 and 2010, providing transects from high northern (~80°N) to high southern latitudes (~70°S), confirms that CH_4 is realistically simulated in the remote troposphere. The deviations seen in the UTLS (NOAA, HIPPO, and CARIBIC aircraft data) are attributed to stratospheric intrusions into the troposphere, which cannot be resolved by the coarse model resolution, but have probably only a relatively small impact on the simulations at the surface (and hence on the inversion results), considering the overall small contribution of the stratospheric sink to the total CH_4 sink.

[61] Comparing the IMAPv5.5 retrievals applied in this study with the previous IMAPv5.0 [*Frankenberg et al*., 2011], as well as independent validation against Total Carbon Column Observing Network (TCCON) Fourier transform spectrometer (FTS) measurements [*Notholt et al*., 2012; *Wunch et al*., 2011], suggests that the IMAPv5.5 retrievals may have a complex bias structure, which may not be adequately compensated by our default polynomial bias correction (applied in (S1-SCIA) - (S4-SCIA)). The alternative smooth bias correction (S5-SCIA) indeed showed significant differences in the derived emissions and their IAV. While performing almost equally against most validation data used in this study, however, S5-SCIA performs worse than (S1-SCIA) - (S4-SCIA) (both in terms of bias and RMS) when compared to independent measurements in the free troposphere over the Amazon, suggesting that the smooth bias correction may not properly disentangle the required bias correction from the emission signal. In a parallel study, the bias of the SCIAMACHY retrievals, and potential alternatives to correct for these biases, is investigated in more detail (S. Houweling et al., manuscript in preparation, 2013). Despite significant dependence on the bias correction of derived emission anomalies on smaller scales, S5-SCIA shows relatively good consistency with (S1-SCIA) - (S4-SCIA), when aggregating the derived IAV of emissions over larger latitude bands.

[62] Significant improvements of future CH_4 inversions are expected from the use of new satellite sensors, such as the Greenhouse Gases Observing Satellite (GOSAT) (in orbit since 2009) which enables XCH_4 retrievals with better accuracy [*Butz et al*., 2011; *Schepers et al*., 2012].

[63] **Acknowledgments.** This work has been supported by the European Commission's Seventh Framework Programme (FP7/2007–2013) projects MACC under grant agreement 218793 and MACC-2 under grant agreement 283576. We are grateful to Philippe Le Sager for preprocessing the ECMWF meteorological data as TM5 input. We thank Greet Janssens-Maenhout for providing the EDGARv4.2 emission inventory and for the helpful comments on the manuscript and Christoph Brühl for providing the stratospheric CH_4 sinks from the ECHAM5/MESSy1 model. We thank ECMWF for providing computing resources under the special projects "Inverse Modelling of Atmospheric CH_4 and N_2O" (2009–2011) and "Global and Regional Inverse Modeling of Atmospheric CH_4 and N_2O" (2012–2014). Aircraft observations over SGP were supported by the Office of Biological and Environmental Research of the U.S. Department of Energy under contract DE-AC02-05CH11231 as part of the Atmospheric Radiation Measurement Program (ARM), ARM Aerial Facility, and Terrestrial Ecosystem Science Program.

References

Aydin, M., K. R. Verhulst, E. S. Saltzman, M. O. Battle, S. A. Montzka, D. R. Blake, Q. Tang, and M. J. Prather (2011), Recent decreases in fossil-fuel emissions of ethane and methane derived from firn air, *Nature*, *476*, 198–201.

Beck, V., et al. (2012), Methane airborne measurements and comparison to global models during BARCA, *J. Geophys. Res.*, *117*, D15310, doi:10.1029/2011JD017345.

Bergamaschi, P., et al. (2007), Satellite chartography of atmospheric methane from SCIAMACHY onboard ENVISAT: (II) Evaluation based on inverse model simulations, *J. Geophys. Res.*, *112*, D02304, doi:10.1029/2006JD007268.

Bergamaschi, P., et al. (2009), Inverse modeling of global and regional CH_4 emissions using SCIAMACHY satellite retrievals, *J. Geophys. Res.*, *114*, D22301, doi:10.1029/2009JD012287.

Bergamaschi, P., et al. (2010), Inverse modeling of European CH_4 emissions 2001–2006, *J. Geophys. Res.*, *115*, D22309, doi:10.1029/2010JD014180.

Biraud, S. C., M. S. Torn, J. R. Smith, C. Sweeney, W. J. Riley, and P. P. Tans (2013), A multi-year record of airborne CO_2 observations in the US. Southern Great Plains, *Atmos. Meas. Tech.*, *6*, 751–763.

Blake, D., and F. Rowland (1988), Continuing worldwide increase in tropospheric methane, *Science*, *239*, 1129–1131.

Bousquet, P., et al. (2006), Contribution of anthropogenic and natural sources to atmospheric methane variability, *Nature*, *443*, doi:10.1038/nature05132.

Bousquet, P., et al. (2011), Source attribution of the changes in atmospheric methane for 2006–2008, *Atmos. Chem. Phys.*, *11*, 3689–3700.

Brenninkmeijer, C. A. M., et al. (2007), Civil Aircraft for the Regular Investigation of the atmosphere Based on an Instrumented Container: The new CARIBIC system, *Atmos. Chem. Phys.*, *7*, 4953–4976.

Brook, E. D., D. Archer, E. Dlugokencky, S. Frolking, and D. M. Lawrence (2008), Potential for abrupt changes in atmospheric methane, in *Abrupt Climate Change*, A report by the U.S. Climate Change Science Program and the Subcommittee on Global Change Research. U.S. Geological Survey, Reston, VA, pp. 258-359.

Butz, A., et al. (2011), Toward accurate CO_2 and CH_4 observations from GOSAT, *Geophys. Res. Lett.*, *38*, L14812, doi:10.1029/2011GL047888.

Chen, H., et al. (2010), High-accuracy continuous airborne measurements of greenhouse gases (CO_2 and CH_4) using the cavity ring-down spectroscopy (CRDS) technique, *Atmos. Meas. Tech.*, *3*, 375–386.

Cunnold, D. M., et al. (2002), In situ measurements of atmospheric methane at GAGE/AGAGE sites during 1985–2000 and resulting inferences, *J. Geophys. Res.*, *107*(D14), 4225, 10.1029/2001JD001226.

Dee, D. P., et al. (2011), The ERA-Interim reanalysis: Configuration and performance of the data assimilation system, *Q. J. R. Meteorol. Soc.*, *137*, 553–597.

Dlugokencky, E. J., L. P. Steele, P. M. Lang, and K. A. Masarie (1994a), The growth rate and distribution of atmospheric methane, *J. Geophys. Res.*, *99*, 17021–17043.

Dlugokencky, E. J., K. A. Masaire, P. M. Lang, P. P. Steele, and E. G. Nisbet (1994b), A dramatic decrease in the growth rate of atmospheric methane in the Northern Hemisphere during 1992, *Geophys. Res. Lett.*, *21*, 45–48.

Dlugokencky, E. J., S. Houweling, L. Bruhwiler, K. A. Masarie, P. M. Lang, J. B. Miller, and P. P. Tans (2003), Atmospheric methane levels off: Temporary pause or a new steady-state? *Geophys. Res. Lett.*, *30*(19), 1992, doi:10.1029/2003GL018126.

Dlugokencky, E. J., R. C. Myers, P. M. Lang, K. A. Masarie, A. M. Crotwell, K. W. Thoning, B. D. Hall, J. W. Elkins, and L. P. Steele (2005), Conversion of NOAA atmospheric dry air CH_4 mole fractions to a gravimetrically prepared standard scale, *J. Geophys. Res.*, *110*, D18306, doi:10.1029/2005JD006035.

Dlugokencky, E. J., et al. (2009), Observational constraints on recent increases in the atmospheric CH_4 burden, *Geophys. Res. Lett.*, *36*, L18803, doi:10.1029/2009GL039780.

Dlugokencky, E. J., E. G. Nisbet, R. Fisher, and D. Lowry (2011), Global atmospheric methane: Budget, changes and dangers, *Phil. Trans. R. Soc. A*, *369*(1943), 2058–2072.

EPA (2012), Global Anthropogenic Non-CO2 Greenhouse Gas Emissions: 1990–2030; Revised December 2012 *Rep.*, U.S. Environmental Protection Agency, Washington, DC 20460.

Etheridge, D. M., L. P. Steele, R. J. Francey, and R. L. Langenfelds (1998), Atmospheric methane between 1000 A.D. and present: Evidence of anthropogenic emissions and climatic variability, *J. Geophys. Res.*, *103*, 15979–15993.

Forster, P., et al. (2007), Changes in atmospheric constituents and in radiative forcing, in *Climate Change 2007: The Physical Science Basis. Contribution of Working Group I to the Fourth Assessment Report of the Intergovernmental Panel on Climate Change*, edited by S. Solomon, D. Qin, M. Manning, Z. Chen, M. Marquis, K. B. Averyt, M. Tignor, and H. L. Miller, Cambridge University Press, Cambridge, United Kingdom and New York, NY, USA, pp. 129-234.

Frankenberg, C., J. F. Meirink, P. Bergamaschi, A. P. H. Goede, M. Heimann, S. Körner, U. Platt, M. van Weele, and T. Wagner (2006), Satellite chartography of atmospheric methane from SCIAMACHY onboard ENVISAT: Analysis of the years 2003 and 2004, *J. Geophys. Res.*, *111*, D07303, doi:10.1029/2005JD006235.

Frankenberg, C., P. Bergamaschi, A. Butz, S. Houweling, J. F. Meirink, J. Notholt, A. K. Petersen, H. Schrijver, T. Warneke, and I. Aben (2008), Tropical methane emissions: A revised view from SCIAMACHY onboard ENVISAT, *Geophys. Res. Lett.*, *35*, L15811, doi:10.1029/2008GL034300.

Frankenberg, C., I. Aben, P. Bergamaschi, E. J. Dlugokencky, R. van Hees, S. Houweling, P. van der Meer, R. Snel, and P. Tol (2011), Global column-averaged methane mixing ratios from 2003–2009 as derived from SCIAMACHY: Trends and variability, *J. Geophys. Res.*, *116*, D04302, doi:10.1029/2010JD014849.

Gilbert, J. C., and C. Lemaréchal (1989), Some numerical experiments with variable-storage quasi-Newton algorithms, *Math. Prog.*, *45*, 407–435.

Hofmann, D. J., J. H. Butler, E. J. Dlugokencky, J. W. Elkins, K. Masarie, S. A. Montzka, and P. Tans (2006), The role of carbon dioxide in climate forcing from 1979–2004: Introduction of the Annual Greenhouse Gas Index, *Tellus*, *58B*, 614–619.

Holmes, C. D., M. J. Prather, O. A. Søvde, and G. Myhre (2013), Future methane, hydroxyl, and their uncertainties: Key climate and emission parameters for future predictions, *Atmos. Chem. Phys.*, *13*, 285–302.

Houweling, S., T. Kaminski, F. Dentener, J. Lelieveld, and M. Heimann (1999), Inverse modeling of methane sources and sinks using the adjoint of a global transport model, *J. Geophys. Res.*, *104*, 26137–26160.

Huijnen, V., et al. (2010), The global chemistry transport model TM5: Description and evaluation of the tropospheric chemistry version 3.0, *Geosci. Model Dev.*, *3*, 445–473.

Jöckel, P., et al. (2006), The atmospheric chemistry general circulation model ECHAM5/MESSy1: Consistent simulation of ozone from the surface to the mesosphere, *Atmos. Chem. Phys.*, *6*, 5067–5104.

JRC/PBL (2011), European Commission, Joint Research Centre (JRC)/Netherlands Environmental Assessment Agency (PBL), Emission Database for Global Atmospheric Research (EDGAR), release version 4.2, http://edgar.jrc.ec.europa.eu.

Kai, F. M., S. C. Tyler, J. T. Randerson, and D. R. Blake (2011), Reduced methane growth rate explained by decreased Northern Hemisphere microbial sources, *Nature*, *476*, 194–197.

Kort, E. A., P. K. Patra, K. Ishijima, B. C. Daube, R. Jiménez, J. Elkins, D. Hurst, F. L. Moore, C. Sweeney, and S. C. Wofsy (2011), Tropospheric distribution and variability of N_2O: Evidence for strong tropical emissions, *Geophys. Res. Lett.*, *38*, L15806, doi:10.1029/2011GL047612.

Kort, E. A., et al. (2012), Atmospheric observations of Arctic Ocean methane emissions up to 82° north, *Nat. Geosci.*, *5*, 318–321.

Krol, M. C., S. Houweling, B. Bregman, M. van den Broek, A. Segers, P. van Velthoven, W. Peters, F. Dentener, and P. Bergamaschi (2005), The two-way nested global chemistry-transport zoom model TM5: Algorithm and applications, *Atmos. Chem. Phys.*, *5*, 417–432.

Krol, M. C., J. F. Meirink, P. Bergamaschi, J. E. Mak, D. Lowe, P. Jöckel, S. Houweling, and T. Röckmann (2008), What can ^{14}CO measurements tell us about OH?, *Atmos. Chem. Phys.*, *8*, 5033–5044.

Lambert, G., and S. Schmidt (1993), Reevaluation of the oceanic flux of methane: Uncertainties and long term variations, *Chem. Global Change Sci.*, *26*(1-4), 579–589.

Langenfelds, R. L., R. J. Francey, B. C. Pak, L. P. Steele, J. Lloyd, C. M. Trudinger, and C. E. Allison (2002), Interannual growth rate variations of atmospheric CO_2 and its $\delta^{13}C$, H_2, CH_4, and CO between 1992 and 1999 linked to biomass burning, *Global Biogeochem. Cycles*, *16*(3), 1048, doi:10.1029/2001GB001466.

Levin, I., C. Veidt, B. H. Vaughn, G. Brailsford, T. Bromley, R. Heinz, D. Lowe, J. B. Miller, C. Poß, and J. W. C. White (2012), No inter-hemispheric $\delta^{13}CH_4$ trend observed, *Nature*, *486*.

Logan, J. A., I. Megretskaia, R. Nassar, L. T. Murray, L. Zhang, K. W. Bowman, H. M. Worden, and M. Luo (2008), Effects of the 2006 El Niño on tropospheric composition as revealed by data from the Tropospheric Emission Spectrometer (TES), *Geophys. Res. Lett.*, *35*, L03816, doi:10.1029/2007GL031698.

Loulergue, L., A. Schilt, R. Spahni, V. Masson-Delmotte, T. Blunier, B. Lemieux, J.-M. Barnola, D. Raynaud, T. F. Stocker, and J. Chappellaz (2008), Orbital and millennial-scale features of atmospheric CH_4 over the past 800,000 years, *Nature*, *453*, 383–386, doi:10.1038/nature06950.

Matthews, E., I. Fung, and J. Lerner (1991), Methane emission from rice cultivation: Geographic and seasonal distribution of cultivated areas and emissions, *Global Biogeochem. Cycles*, *5*, 3–24.

Meirink, J. F., P. Bergamaschi, and M. Krol (2008), Four-dimensional variational data assimilation for inverse modelling of atmospheric methane emissions: Method and comparison with synthesis inversion, *Atmos. Chem. Phys.*, *8*, 6341–6353.

Montzka, S. A., M. Krol, E. Dlugokencky, B. Hall, P. Jöckel, and J. Lelieveld (2011), Small interannual variability of global atmospheric hydroxyl, *Science*, *331*, 67–69.

Notholt, J., T. Blumenstock, D. Brunner, B. Buchmann, B. Dils, M. De Mazière, C. Popp, and R. Sussmann (2012), ESA Climate Change Initiative (CCI): Product Validation and Algorithm Selection Report (PVASR) for the Essential Climate Variable (ECV) Greenhouse Gases (GHG) Technical Report, 22 August 2012, available from http://www.esa-ghg-cci.org.

Patra, P. K., et al. (2011), TransCom model simulations of CH_4 and related species: Linking transport, surface flux and chemical loss with CH_4 variability in the troposphere and lower stratosphere, *Atmos. Chem. Phys.*, *11*, 12813–12837.

Peters, W., et al. (2007), An atmospheric perspective on North American carbon dioxide exchange: CarbonTracker, *Proc. Natl. Acad. Sci. U. S. A.*, *104*(48), 18925–18930.

Prather, M., M. McElroy, S. Wofsy, G. Russel, and D. Rind (1987), Chemistry of the global troposphere: Fluorocarbons as tracers of air motion, *J. Geophys. Res.*, *92*, 6579–6613.

Ridgwell, A. J., S. J. Marshall, and K. Gregson (1999), Consumption of atmospheric methane by soils: A process-based model, *Global Biogeochem. Cycles*, *13*, 59–70, doi:10.1029/1998GB900004.

Rigby, M., et al. (2008), Renewed growth of atmospheric methane, *Geophys. Res. Lett.*, *35*, L22805, doi:10.1029/2008GL036037.

Sanderson, M. G. (1996), Biomass of termites and their emissions of methane and carbon dioxide: A global database, *Global Biogeochem. Cycles*, *10*, 543–557.

Schepers, D., et al. (2012), Methane retrievals from Greenhouse Gases Observing Satellite (GOSAT) shortwave infrared measurements: Performance comparison of proxy and physics retrieval algorithms, *J. Geophys. Res.*, *117*, D10307, doi:10.1029/2012JD017549.

Schuck, T. J., C. A. M. Brenninkmeijer, A. K. Baker, F. Slemr, P. F. J. van Velthoven, and A. Zahn (2010), Greenhouse gas relationships in the Indian summer monsoon plume measured by the CARIBIC passenger aircraft, *Atmos. Chem. Phys.*, *10*, 3965–3984.

Schuck, T. J., K. Ishijima, P. K. Patra, A. K. Baker, T. Machida, H. Matsueda, Y. Sawa, T. Umezawa, C. A. M. Brenninkmeijer, and J. Lelieveld (2012), Distribution of methane in the tropical upper troposphere measured by CARIBIC and CONTRAIL aircraft, *J. Geophys. Res.*, *117*, D19304, doi:10.1029/2012JD018199.

Shakhova, N., I. Semiletov, A. Salyuk, V. Yusupov, D. Kosmach, and Ö. Gustafsson (2010), Extensive methane venting to the atmosphere from sediments of the East Siberian Arctic Shelf, *Science*, *327*, 246–1250.

Shindell, D. T., G. Faluvegi, N. Bell, and G. Schmidt (2005), An emissions based view of climate forcing by methane and tropospheric ozone, *Geophys. Res. Lett.*, *32*, L04803, doi:10.1029/2004GL021900.

Shindell, D., et al. (2012), Simultaneously mitigating near-term climate change and improving human health and food security, *Science*, *335*, 183–189.

Simpson, I. J., F. S. Rowland, S. Meinardi, and D. R. Blake (2006), Influence of biomass burning during recent fluctuations in the slow growth of global tropospheric methane, *Geophys. Res. Lett.*, *33*, L22808, doi:10.1029/2006GL027330.

Simpson, I. J., M. P. Sulbaek Andersen, S. Meinardi, L. Bruhwiler, N. J. Blake, D. Helmig, F. S. Rowland, and D. R. Blake (2012), Long-term decline of global atmospheric ethane concentrations and implications for methane, *Nature*, *488*.

Spahni, R., et al. (2005), Atmospheric methane and nitrous oxide of the late Pleistocene from Antarctic ice cores, *Science*, *310*, 1317–1321.

Spahni, R., et al. (2011), Constraining global methane emissions and uptake by ecosystems, *Biogeosci.*, *8*, 1643–1665.

Spivakovsky, C. M., et al. (2000), Three-dimensional climatological distribution of tropospheric OH: Update and evaluation, *J. Geophys. Res.*, *105*, 8931–8980.

Walter Anthony, K. M., P. Anthony, G. Grosse, and J. Chanton (2012), Geologic methane seeps along boundaries of Arctic permafrost thaw and melting glaciers, *Nat. Geosci.*, *5*, 419–426.

van der Werf, G. R., J. T. Randerson, L. Giglio, G. J. Collatz, M. Mu, P. S. Kasibhatla, D. C. Morton, R. S. DeFries, Y. Jin, and T. T. van Leeuwen (2010), Global fire emissions and the contribution of deforestation, savanna, forest, agricultural, and peat fires (1997–2009), *Atmos. Chem. Phys.*, *10*, 11707–11735.

Wofsy, S. C. (2011), HIAPER Pole-to-Pole Observations (HIPPO): Fine-grained, global-scale measurements of climatically important atmospheric gases and aerosols, *Phil. Trans. R. Soc. A*, *369*, 2073–2086.

Worden, J., K. Wecht, C. Frankenberg, M. Alvarado, K. Bowman, E. Kort, S. Kulawik, M. Lee, V. Payne, and H. Worden (2013), CH_4 and CO distributions over tropical fires during October 2006 as observed by the Aura TES satellite instrument and modeled by GEOS-Chem, *Atmos. Chem. Phys.*, *13*, 3679–3692.

Wunch, D., G. C. Toon, J.-F. L. Blavier, R. A. Washenfelder, J. Notholt, B. J. Connor, D. W. T. Griffith, V. Sherlock, and P. O. Wennberg (2011), The Total Carbon Column Observing Network, *Phil. Trans. R. Soc. A*, *369*, 2087–2112.

Yurganov, L. N., et al. (2005), Increased Northern Hemispheric carbon monoxide burden in the troposphere in 2002 and 2003 detected from the ground and from space, *Atmos. Chem. Phys.*, *5*, 563–573.